VEM-Nitsche fully discrete polytopal scheme for frictionless contact-mechanics

Mohamed Laaziri, Roland Masson

VEM–Nitsche fully discrete polytopal scheme for frictionless contact-mechanics

Mohamed Laaziri*[1] and Roland Masson†[1]

[1]Université Côte d'Azur, Inria, CNRS, Laboratoire J.A. Dieudonné, team Galets, Nice, France

Abstract

This work targets the discretisation of contact-mechanics accounting for small strains, linear elastic constitutive laws, and fractures or faults represented as a network of co-dimension one planar interfaces. This type of models coupled with Darcy flow plays an important role typically for the simulation of fault reactivation by fluid injection in geological storages or the hydraulic fracture stimulation in enhanced geothermal systems. To simplify the presentation, a frictionless contact behavior at matrix fracture interfaces is considered, although the scheme developed in this work readily extends to more complex contact models such as the Mohr-Coulomb friction. To account for the geometrical complexity of subsurface, our discretisation is based on the first order Virtual Element Method (VEM) which generalises the $\mathbb{P}_1$ finite element method to polytopal meshes. Following previous works in the finite element framework, the contact conditions are enforced in a weak sense using Nitsche's formulation based on additional consistent penalization terms. We perform, in a fully discrete framework, the well-posedness and convergence analysis showing an optimal first order error estimate with minimal regularity assumptions. Numerical experiments confirm our theoretical findings and exhibit the good behavior of the nonlinear semi-smooth Newton solver.

Keywords: Polytopal method, Virtual Element Method, Nitsche's method, Fully discrete approach, Error estimates, Contact-mechanics, Fracture networks, Poromechanics.

1 Introduction

The simulation of poromechanical models in fractured (or faulted) porous rocks plays an important role in many subsurface applications such as fault reactivation by fluid injection in geological storages or the hydraulic fracture stimulation in deep geothermal systems. One of the key difficulty to simulate such models is the discretisation of the contact-mechanical model which must be adapted to geological meshes. This motivates the use of polytopal discretisations to cope with the complexity of the geometries representing geological structures including faults/fractures, layering, erosions and heterogeneities.

Different classes of polytopal methods have been developed in the field of mechanics such as Discontinuous Galerkin [34], Hybrid High Order (HHO) [26], MultiPoint Stress Approximation (MPSA) [38], Hybrid Mimetic Methods [25] and Virtual Element Methods (VEM) [6, 5, 7]. Some of them have been extended to account for contact-mechanics as in [9] for

*Corresponding author, mohamed.laaziri@univ-cotedazur.fr
†Corresponding author, roland.masson@univ-cotedazur.fr

the MSPA based on face-wise constant approximations of the surface tractions and displacement jump along the fracture network, in [18] for HHO combined with a Nitsche's contact formulation, in [44, 23] for VEM based on node to node contact conditions, and in [41, 45] for the VEM method combined with a primal variational inequality formulation. Among these polytopal methods, VEM, as a natural extension of the Finite Element Method (FEM) to polyhedral meshes, has received a lot of attention in the mechanics community since its introduction in [5] and has been applied to various problems including in the context of geomechanics [2], poromechanics [24, 11, 31] and fracture mechanics [43].

Another key feature of subsurface applications of contact-mechanical models is the choice of the contact formulation which must be able to deal with network of fractures including corners, tips and intersections. This raises difficulties for nodal based contact conditions and has motivated the use of mixed formulations with face-wise constant Lagrange multipliers as in [8, 30, 33, 10] in the Finite Element framework. This approach enables the handling of fracture networks and the use of efficient semi-smooth Newton nonlinear solvers. It has been recently extended to the VEM framework in [28]. On the other hand, the combination of a first order nodal discretisation of the displacement field with a face-wise constant approximation of the Lagrange multiplier requires a stabilisation to ensure the inf-sup compatibility condition. This is achieved in [28] by extending to the polytopal framework the $\mathbb{P}^1$-bubble FEM discretisation [8] based on the enrichment of the displacement space by an additional bubble unknown on one side of each fracture face.

Another key feature of subsurface applications of contact-mechanical models is the choice of the contact formulation which must be able to deal with network of fractures including corners, tips and intersections. This raises difficulties for nodal based contact conditions and has motivated the investigation of various formulations such as Mortar methods (see [42] and the references there-in), mixed and stabilised mixed methods [35, 42, 40, 36], and augmented Lagrangian methods [1, 16, 15]. Mixed formulations with face-wise constant Lagrange multipliers, as in [8, 30, 33, 10] in the Finite Element framework, are particularly well-suited to deal with complex networks of fractures and lead to efficient semi-smooth Newton nonlinear solvers. This type of discretisation has been recently extended to the VEM framework in [28]. On the other hand, the combination of a first order nodal discretisation of the displacement field with a face-wise constant approximation of the Lagrange multiplier requires a stabilisation to ensure the inf-sup compatibility condition. This is achieved in [28] by extending to the polytopal framework the $\mathbb{P}^1$-bubble FEM discretisation [8] based on the enrichment of the displacement space by an additional bubble unknown on one side of each fracture face.

In this work, we investigate an alternative approach based on the Nitsche's formulation of contact-mechanics introduced in [19, 21, 17, 20] in the Finite Element framework. Nitsche's method formulates the contact condition in a weak sense by appropriate consistent penalisation terms that involve only the primal displacement unknown. Moreover, no additional unknown (Lagrange multiplier) is needed and, therefore, no discrete inf–sup condition must be fulfilled, contrarily to mixed methods. It is naturally suited to semi-smooth Newton nonlinear solvers and readily deals with network of fractures. The first polytopal discretisation of contact mechanics using Nitsche's method is developed and analysed in [18] based on the HHO scheme with cell and face unknowns. However, to the best of our knowledge, the extension of Nitsche's technique to the nodal VEM framework has not been yet derived nor analysed.

The objective of this work is to introduce and analyse the first order VEM Nitsche's for-

mulation of contact-mechanics considering small strains hypothesis and a linear elastic constitutive law. For simplicity, the discretisation and the convergence analysis is presented for a frictionless contact model but the scheme readily extends to the Coulomb frictional model and the numerical analysis to the Tresca frictional model following [17, 20, 3]. The VEM Nitsche's discretisation is introduced based on a fully discrete framework with vector space of discrete unknowns and reconstruction operators in the spirit of HHO discretisation [26]. The numerical analysis combines techniques developed in [19, 21] for the Nitsche's method together with those of [29] for non conforming discretisations in a fully discrete framework. It leads to an optimal first order error estimate with minimal regularity assumption which readily extends to the Tresca frictional model.

The remaining of this paper is organised as follows. Section 2 introduces the static contact-mechanical model with frictionless contact conditions. Section 3 introduces the main ingredients of the discretisation with the mesh described in Section 3.1, the discrete displacement space in Section 3.2, the function, jump, normal traction, and gradient reconstruction operators in Section 3.3, the definition of the interpolation operator in Section 3.5, and Nitsche's formulation in Section 3.6. Section 4 performs the well-posedness and convergence analysis of the scheme and Section 5 investigates the numerical behavior of the scheme in order to assess our theoretical results. We first consider a 3D manufactured analytical solution with a single fracture from [28] to check numerically the error estimate. Then, we consider a more challenging 3D Discrete Fracture Matrix model with Coulomb frictional contact. We first study the sensitivity of Nitsche's method to its parameters. Then, we compare the VEM Nitsche's discretisation with the VEM-bubble method introduced in [28] both in terms of accuracy of the solution using a fine mesh reference solution and in terms of robustness of the nonlinear solver.

2 Contact-mechanical Model

We let $\Omega \subset \mathbb{R}^d$, $d = 3$, denote a bounded polyhedral domain, partitioned into a fracture domain Γ and a matrix domain $\Omega \backslash \overline{\Gamma}$. The network of fractures is defined by

$$\overline{\Gamma} = \bigcup_{i \in I} \overline{\Gamma}_i,$$

where each fracture $\Gamma_i \subset \Omega$, $i \in I$ is a planar polygonal simply connected open domain. Without restriction of generality, we will assume that the fractures may only intersect at their boundaries, that is, for any $i, j \in I, i \neq j$ it holds $\Gamma_i \cap \Gamma_j = \emptyset$, but not necessarily $\overline{\Gamma}_i \cap \overline{\Gamma}_j = \emptyset$.

The two sides of a given fracture of Γ are denoted by $\pm$ in the matrix domain, with unit normal vectors $\mathbf{n}^{\pm}$ oriented outward from the sides $\pm$ such that $\mathbf{n}^+ + \mathbf{n}^- = \mathbf{0}$. We denote by $\gamma_{\mathfrak{a}}$ the trace operators on the side $\mathfrak{a} \in \{+, -\}$ of Γ for functions in $H^1(\Omega \backslash \overline{\Gamma})$. The jump operator on Γ for functions $\mathbf{u}$ in $H^1(\Omega \backslash \overline{\Gamma})^d$ is defined by

$$[\![\mathbf{u}]\!] = \gamma_+ \mathbf{u} - \gamma_- \mathbf{u},$$

and we denote by $[\![\mathbf{u}]\!]_{\mathbf{n}} = [\![\mathbf{u}]\!] \cdot \mathbf{n}^+$ its normal component. The normal trace operator on the side $\mathfrak{a} \in \{+, -\}$ of Γ oriented outward to the side $\mathfrak{a}$, applied to $H_{\mathrm{div}}(\Omega \backslash \overline{\Gamma})$ functions is denoted by $\gamma_{\mathbf{n}}^{\mathfrak{a}}$.

The symmetric gradient operator $\boldsymbol{\epsilon}$ is defined such that $\boldsymbol{\epsilon}(\mathbf{v}) = \frac{1}{2}(\nabla \mathbf{v} + {}^T \nabla \mathbf{v})$ for a given vector field $\mathbf{v} \in H^1(\Omega \backslash \overline{\Gamma})^d$.

Given for simplicity homogeneous Dirichlet boundary conditions, the space for the displacement is

$$\mathbf{U}_0 = H_0^1(\Omega\backslash\overline{\Gamma})^d,$$

endowed with the semi-norm $\|\mathbf{v}\|_{\mathbf{U}_0} = \|\nabla\mathbf{v}\|_{L^2(\Omega)^d}$ which defines a norm on $\mathbf{U}_0$ assuming that $\Omega\backslash\overline{\Gamma}$ is connected.

The model accounts for the mechanical equilibrium equation with a linear elastic constitutive law and a frictionless contact model at matrix–fracture interfaces. In its strong form, it is defined by the following system of partial differential equations:

$$\begin{cases} -\mathbf{div}\boldsymbol{\sigma}(\mathbf{u}) = \mathbf{f} & \text{on } \Omega\backslash\overline{\Gamma}, \\ \boldsymbol{\sigma}(\mathbf{u}) = \mathbb{A}\boldsymbol{\epsilon}(\mathbf{u}) & \text{on } \Omega\backslash\overline{\Gamma}, \\ \gamma_{\mathbf{n}}^+(\boldsymbol{\sigma}(\mathbf{u})) + \gamma_{\mathbf{n}}^-(\boldsymbol{\sigma}(\mathbf{u})) = 0 & \text{on } \Gamma, \\ \sigma_{\mathbf{n}}(\mathbf{u}) \leqslant 0,\ [\![\mathbf{u}]\!]_{\mathbf{n}} \leqslant 0,\ [\![\mathbf{u}]\!]_{\mathbf{n}}\sigma_{\mathbf{n}}(\mathbf{u}) = 0 & \text{on } \Gamma, \\ \boldsymbol{\sigma}_{\boldsymbol{\tau}}(\mathbf{u}) = 0, & \text{on } \Gamma, \end{cases} \tag{1}$$

with $\mathbb{A}$ the fourth order symmetric elasticity tensor having the usual uniform ellipticity and boundedness property, and the normal and tangential surface tractions defined by

$$\begin{cases} \sigma_{\mathbf{n}}(\mathbf{u}) = \gamma_{\mathbf{n}}^+(\boldsymbol{\sigma}(\mathbf{u}))\cdot\mathbf{n}^+ & \text{on } \Gamma, \\ \boldsymbol{\sigma}_{\boldsymbol{\tau}}(\mathbf{u}) = \gamma_{\mathbf{n}}^+(\boldsymbol{\sigma}(\mathbf{u})) - \sigma_{\mathbf{n}}(\mathbf{u})\mathbf{n}^+ & \text{on } \Gamma. \end{cases} \tag{2}$$

The model (1) is formulated in mixed form using a Lagrange multiplier $\lambda : \Gamma \to \mathbb{R}$ at matrix–fracture interfaces. Define the normal displacement jump space by

$$W_{\Gamma,\mathbf{n}} = \{[\![\mathbf{v}]\!]_{\mathbf{n}} \,:\, \mathbf{v} \in \mathbf{U}_0\}$$

and denote by $W'_{\Gamma,\mathbf{n}}$ its dual space; the duality pairing between these two spaces is written $\langle\cdot,\cdot\rangle_\Gamma$. The dual cone is then defined by

$$C_f = \Big\{\mu \in W'_{\Gamma,\mathbf{n}} \,:\, \langle\mu, v\rangle_\Gamma \leq 0 \text{ for all } v \in W_{\Gamma,\mathbf{n}} \text{ with } v \leq 0\Big\}.$$

The weak mixed-variational formulation for adressing the problem (1) reads: find $\mathbf{u} \in \mathbf{U}_0$ and $\lambda \in C_f$ such that for all $\mathbf{v} \in \mathbf{U}_0$ and $\mu \in C_f$, one has

$$\int_\Omega \boldsymbol{\sigma}(\mathbf{u}) : \boldsymbol{\epsilon}(\mathbf{v}) + \langle\lambda, [\![\mathbf{v}]\!]_{\mathbf{n}}\rangle_\Gamma = \int_\Omega \mathbf{f}\cdot\mathbf{v}, \tag{3a}$$

$$\langle\mu - \lambda, [\![\mathbf{u}]\!]_{\mathbf{n}}\rangle_\Gamma \leq 0. \tag{3b}$$

It is well known that this problem admits a unique solution $(\mathbf{u},\lambda) \in \mathbf{U}_0 \times W'_{\Gamma,\mathbf{n}}$ (see e.g. [22]). Note that, based on the variational formulation, the Lagrange multiplier satisfies $\lambda = -\sigma_{\mathbf{n}}(\mathbf{u})$, and that, assuming $\sigma_{\mathbf{n}}(\mathbf{u}) \in L^2(\Gamma)$, one has

$$\sigma_{\mathbf{n}}(\mathbf{u}) = [P_\beta(\mathbf{u})]_{\mathbb{R}^-}, \tag{4}$$

with $[a]_{\mathbb{R}^-} = \min(a, 0)$, where P_β is the linear operator such that

$$P_\beta(\mathbf{u}) = \sigma_{\mathbf{n}}(\mathbf{u}) - \beta[\![\mathbf{u}]\!]_n,$$

and $\beta \in L^\infty(\Gamma)$ is any given strictly positive function.

3 Discretisation

This Section introduces the discretisation of the contact-mechanical model (1) based on nodal unknowns accounting for the discontinuity of the displacement field at matrix fracture interfaces. The presentation of the scheme is done in a fully discrete framework with vector space of discrete unknowns and reconstruction operators. Proceeding as in Section 3.4 of [28] it can be shown to be equivalent to a VEM formulation based on the same displacement degrees of freedom [5]. The scheme can therefore be interpreted as a $\mathbb{P}_1$ VEM Nitsche's discretisation.

3.1 Mesh

We consider a polyhedral mesh of the domain Ω assumed to be conforming with the fracture network Γ. For each cell K (resp. face σ), we denote by h_K (resp. h_σ) and $|K|$ (resp. $|\sigma|$) its diameter and its measure, and we set

$$h_{\mathcal{D}} = \max_{K\in\mathcal{M}} h_K.$$

The set of cells K, the set of faces σ, the set of nodes s and the set of edges e are denoted respectively by $\mathcal{M}$, $\mathcal{F}$, $\mathcal{V}$ and $\mathcal{E}$. It is assumed that there exists a subset of faces $\mathcal{F}_\Gamma \subset \mathcal{F}$ such that

$$\overline{\Gamma} = \bigcup_{\sigma\in\mathcal{F}_\Gamma} \overline{\sigma}.$$

We denote by $\mathcal{M}_\sigma$ the set of cells neighboring a face $\sigma \in \mathcal{F}$; thus, $\mathcal{M}_\sigma = \{K, L\}$ for interior face $\sigma \in \mathcal{F}^{\rm int}$ (in which case we write $\sigma = K|L$) and $\mathcal{M}_\sigma = \{K\}$ for boundary face $\sigma \in \mathcal{F}^{\rm ext}$. Since $\Gamma \subset \Omega$, we have $\mathcal{F}_\Gamma \subset \mathcal{F}^{\rm int}$. For a face $\sigma \in \mathcal{F}_\Gamma$, K and L in the notation $\sigma = K|L$ are labelled such that $\mathbf{n}_{K\sigma} = \mathbf{n}^+$ and $\mathbf{n}_{L\sigma} = \mathbf{n}^-$, where $\mathbf{n}_{K\sigma}$ (resp. $\mathbf{n}_{L\sigma}$) is the unit normal vector to σ oriented outward of K (resp. L). We denote by $\mathcal{V}^{\rm ext}$ the set of boundary nodes. We denote by $\mathcal{V}_\sigma$ the set of nodes of σ, $\mathcal{E}_\sigma$ the set of edges of σ, by $\mathcal{F}_K$ the set of faces of K, by $\mathcal{V}_K$ the set of nodes of K. For each $\sigma \in \mathcal{F}$, we denote by $\mathbf{n}_{\sigma e}$ the unit normal vector to $e \in \mathcal{E}_\sigma$ in the plane σ oriented outward to σ.

Throughout this paper we suppose that mesh regularity assumptions of [26, Definition 1.9] hold, and we write $a \lesssim b$ (resp. $a \gtrsim$) as a shorthand for $a \le Cb$ (resp. $Ca \le b$) with $C > 0$ depending only on Ω, Γ, on the mesh regularity parameter, and possibly on the elasticity tensor and $\mathbf{f}$.

If $X \in \mathcal{M} \cup \mathcal{F}$ and $\ell \in \mathbb{N}$, we denote by $\mathbb{P}^\ell(X)$ the space of polynomials of degree $\le \ell$ on X. For $\mathcal{X} = \mathcal{M}$ or $\mathcal{X} = \mathcal{F}_\Gamma$, we use the notation $\mathbb{P}^\ell(\mathcal{X})$ for the space of piecewise-polynomials of degree $\le \ell$ on $\mathcal{X}$.

In the following, we denote by $H^2(\mathcal{M})$ (resp. $H^1(\mathcal{F}_\Gamma)$) the space of functions defined on Ω that are H^2 on each $K \in \mathcal{M}$ (resp. defined on Γ and H^1 on each $\sigma \in \mathcal{F}_\Gamma$). These spaces are endowed with their usual broken semi-norms.

3.2 Discrete space

The degrees of freedom (DOFs) for the displacement are nodal (attached to the vertices of the mesh), but could be discontinuous across the fracture network (see Figure 1). To be more specific, let us first define a partition $\overline{\mathcal{M}_s}$ of the set of cells $\mathcal{M}_s$ around a given node $s \in \mathcal{V}$. For a given cell $K \in \mathcal{M}_s$ we denote by $\mathcal{K}s \in \overline{\mathcal{M}_s}$ the subset of $\mathcal{M}_s$ such that $\bigcup_{L\in\mathcal{K}s} \overline{L}$ is the closure of the connected component of $(\bigcup_{L\in\mathcal{M}_s} \overline{L}) \setminus \Gamma$ containing the cell K.

In other words, $\mathcal{K}s$ is the set of cells in $\mathcal{M}_s$ that are on the same side of Γ as K. A nodal displacement unknown $\mathbf{v}_{\mathcal{K}s}$ is defined for each $\mathcal{K}s \in \overline{\mathcal{M}}_s$. Let us note that there is a unique nodal displacement unknown $\mathbf{v}_{\mathcal{K}s}$ at a node s not belonging to Γ, since $\overline{\mathcal{M}}_s = \mathcal{M}_s$ in that case. On the other hand, for a fracture node s, the nodal displacement unknown $\mathbf{v}_{\mathcal{K}s}$ is the one on the side K of the set of fractures connected to s.

The discrete space of displacements, accounting for the possible discontinuities across the fracture network and for the zero boundary condition on $\partial\Omega$, is

$$\mathbf{U}_{0,\mathcal{D}} = \Big\{ \mathbf{v}_{\mathcal{D}} = (\mathbf{v}_{\mathcal{K}s})_{\mathcal{K}s \in \overline{\mathcal{M}}_s, s \in \mathcal{V}} \,:\, \mathbf{v}_{\mathcal{K}s} \in \mathbb{R}^d \,,\ \mathbf{v}_{\mathcal{K}s} = \mathbf{0} \text{ if } s \in \mathcal{V}^{\rm ext} \Big\}. \tag{5}$$

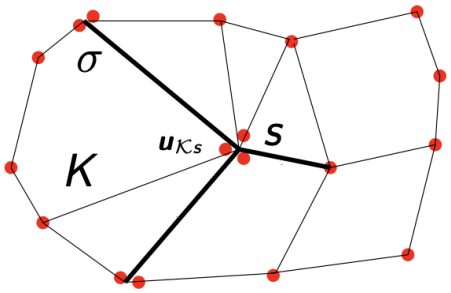

Figure 1: Example of a 2D polygonal mesh with three fracture faces in bold lines and the nodal DOFs at red dots. The displacement unknown at node $\mathbf{s}$ on the cell K side is denoted by $\mathbf{u}_{\mathcal{K}s}$.

3.3 Reconstruction operators in $\mathbf{U}_{0,\mathcal{D}}$

We first define, for each $K \in \mathcal{M}$ and $\sigma \in \mathcal{F}_K$, a tangential face gradient $\nabla^{K\sigma} : \mathbf{U}_{0,\mathcal{D}} \to \mathbb{P}^0(\sigma)^{d\times d}$ and tangential displacement reconstruction $\Pi^{K\sigma} : \mathbf{U}_{0,\mathcal{D}} \to \mathbb{P}^1(\sigma)^d$. First, we choose nonnegative weights $(\omega_s^\sigma)_{s\in\mathcal{V}_\sigma}$ to express the center of mass $\overline{\mathbf{x}}_\sigma$ of σ in terms of that of its vertices:

$$\overline{\mathbf{x}}_\sigma = \sum_{s\in\mathcal{V}_\sigma} \omega_s^\sigma \mathbf{x}_s \,, \quad \sum_{s\in\mathcal{V}_\sigma} \omega_s^\sigma = 1. \tag{6}$$

Then, for $\mathbf{v}_{\mathcal{D}} \in \mathbf{U}_{0,\mathcal{D}}$, we set

$$\begin{aligned} \nabla^{K\sigma}\mathbf{v}_{\mathcal{D}} &= \frac{1}{|\sigma|} \sum_{e=s_1s_2\in\mathcal{E}_\sigma} |e| \frac{\mathbf{v}_{\mathcal{K}s_1} + \mathbf{v}_{\mathcal{K}s_2}}{2} \otimes \mathbf{n}_{\sigma e}, \\ \Pi^{K\sigma}\mathbf{v}_{\mathcal{D}}(\mathbf{x}) &= \nabla^{K\sigma}\mathbf{v}_{\mathcal{D}}(\mathbf{x} - \overline{\mathbf{x}}_\sigma) + \overline{\mathbf{v}}_{K\sigma} \quad \forall \mathbf{x} \in \sigma, \qquad \text{where } \overline{\mathbf{v}}_{K\sigma} = \sum_{s\in\mathcal{V}_\sigma} \omega_s^\sigma \mathbf{v}_{\mathcal{K}s}. \end{aligned} \tag{7}$$

Above, we have noted $e = s_1s_2$ to indicate that the edge e has vertices s_1, s_2.

If $\sigma \in \mathcal{F}_\Gamma$ is a fracture face, and K (resp. L) is the cell on the positive (resp. negative) side of σ, we define the normal displacement jump operator on σ as $[\![\cdot]\!]_{\sigma,\mathbf{n}} : \mathbf{U}_{0,\mathcal{D}} \to \mathbb{P}^1(\sigma)$ such that, for all $\mathbf{v}_{\mathcal{D}} \in \mathbf{U}_{0,\mathcal{D}}$,

$$[\![\mathbf{v}_{\mathcal{D}}]\!]_{\sigma,\mathbf{n}} = (\Pi^{K\sigma}\mathbf{v}_{\mathcal{D}} - \Pi^{L\sigma}\mathbf{v}_{\mathcal{D}}) \cdot \mathbf{n}_{K\sigma}. \tag{8}$$

For each cell $K \in \mathcal{M}$, we select nonnegative weights $(\omega_s^K)_{s\in\mathcal{V}_K}$ of a linear decomposition of the center of mass $\overline{\mathbf{x}}_K$ of K in terms of its vertices

$$\overline{\mathbf{x}}_K = \sum_{s\in\mathcal{V}_K} \omega_s^K \mathbf{x}_s \,, \quad \sum_{s\in\mathcal{V}_K} \omega_s^K = 1,$$

and we constrict a gradient reconstruction $\nabla^K : \mathbf{U}_{0,\mathcal{D}} \to \mathbb{P}^0(K)^{d\times d}$ and a displacement reconstruction $\Pi^K : \mathbf{U}_{0,\mathcal{D}} \to \mathbb{P}^1(K)^d$ by setting, for $\mathbf{v}_\mathcal{D} \in \mathbf{U}_{0,\mathcal{D}}$,

$$\nabla^K \mathbf{v}_\mathcal{D} = \frac{1}{|K|} \sum_{\sigma\in\mathcal{F}_K} |\sigma| \overline{\mathbf{v}}_{K\sigma} \otimes \mathbf{n}_{K\sigma}, \tag{9}$$

$$\Pi^K \mathbf{v}_\mathcal{D}(\mathbf{x}) = \nabla^K \mathbf{v}_\mathcal{D}(\mathbf{x} - \overline{\mathbf{x}}_K) + \overline{\mathbf{v}}_K \quad \forall \mathbf{x} \in K \qquad \text{where } \overline{\mathbf{v}}_K = \sum_{s\in\mathcal{V}_K} \omega_s^K \mathbf{v}_{\mathcal{K}s}. \tag{10}$$

These local normal jump, gradient and displacement reconstructions are patched together to create their global piecewise polynomial counterparts $[\![\cdot]\!]_{\mathcal{D},\mathbf{n}} : \mathbf{U}_{0,\mathcal{D}} \to \mathbb{P}^1(\mathcal{F}_\Gamma)$, $\nabla^\mathcal{D} : \mathbf{U}_{0,\mathcal{D}} \to \mathbb{P}^0(\mathcal{M})^{d\times d}$ and $\Pi^\mathcal{D} : \mathbf{U}_{0,\mathcal{D}} \to \mathbb{P}^1(\mathcal{M})^d$: for all $\mathbf{v}_\mathcal{D} \in \mathbf{U}_{0,\mathcal{D}}$,

$$\begin{aligned}
([\![\mathbf{v}_\mathcal{D}]\!]_{\mathcal{D},\mathbf{n}})_{|\sigma} &= [\![\mathbf{v}_\mathcal{D}]\!]_{\sigma,\mathbf{n}} \quad \forall \sigma \in \mathcal{F}_\Gamma,\\
(\nabla^\mathcal{D} \mathbf{v}_\mathcal{D})_{|K} &= \nabla^K \mathbf{v}_\mathcal{D} \quad \forall K \in \mathcal{M},\\
(\Pi^\mathcal{D} \mathbf{v}_\mathcal{D})_{|K} &= \Pi^K \mathbf{v}_\mathcal{D} \quad \forall K \in \mathcal{M}.
\end{aligned}$$

We also define the cellwise constant reconstruction operator $\widetilde{\Pi}^\mathcal{D} \mathbf{v}_\mathcal{D} : \mathbf{U}_{0,\mathcal{D}} \to \mathbb{P}^0(\mathcal{M})^d$ such that $(\widetilde{\Pi}^\mathcal{D} \mathbf{v}_\mathcal{D})_{|K} = \overline{\mathbf{v}}_K$. Finally, the discrete symmetric gradient $\boldsymbol{\epsilon}_\mathcal{D}$, and stress tensor $\boldsymbol{\sigma}_\mathcal{D}$ are deduced from the previous operators:

$$\boldsymbol{\epsilon}_\mathcal{D} = \frac{1}{2}(\nabla^\mathcal{D} + {}^T\nabla^\mathcal{D}), \quad \text{and} \quad \boldsymbol{\sigma}_\mathcal{D}(\cdot) = \mathbb{A}\boldsymbol{\epsilon}_\mathcal{D}(\cdot).$$

3.4 Stabilisation bilinear form

Except in the case of simplectic cells, the affine function reconstruction $\Pi^K \mathbf{u}_\mathcal{D}$ cannot control all the cell nodal unknowns $\mathbf{u}_{\mathcal{K}s}$, for $s \in \mathcal{V}_K$. Following the VEM approach [6, 5, 7], this motivates the definition of a local stabilisation bilinear form $S_K : \mathbf{U}_{0,\mathcal{D}} \times \mathbf{U}_{0,\mathcal{D}} \to \mathbb{R}$ given for each $K \in \mathcal{M}$ by

$$S_K(\mathbf{u}_\mathcal{D}, \mathbf{v}_\mathcal{D}) = h_K^{d-2} \sum_{s\in\mathcal{V}_K} \left(\mathbf{u}_{K_s} - \Pi^K \mathbf{u}_\mathcal{D}(\mathbf{x}_s)\right) \cdot \left(\mathbf{v}_{K_s} - \Pi^K \mathbf{v}_\mathcal{D}(\mathbf{x}_s)\right), \tag{11}$$

leading to the definition the scaled global stabilisation bilinear form

$$S_{\mu,\lambda,\mathcal{D}}(\mathbf{u}_\mathcal{D}, \mathbf{v}_\mathcal{D}) = \sum_{K\in\mathcal{M}} \mathrm{A}_K S_K(\mathbf{u}_\mathcal{D}, \mathbf{v}_D), \tag{12}$$

where $\mathrm{A}_K = \frac{1}{|K|} \max_{i,j,k,l} \int_K \mathbb{A}_{i,j,k,l} d\mathbf{x}$. We also introduce the unscaled global stabilisation bilinear form

$$S_\mathcal{D}(\mathbf{u}_\mathcal{D}, \mathbf{v}_\mathcal{D}) = \sum_{K\in\mathcal{M}} S_K(\mathbf{u}_\mathcal{D}, \mathbf{v}_D). \tag{13}$$

3.5 Interpolator

The space $\mathcal{C}_0^0(\overline{\Omega}\backslash\Gamma)$ is spanned by functions that are continuous on $\overline{\Omega}\backslash\Gamma$, have limits on each side of Γ, and vanish on $\partial\Omega$. The interpolator $\mathcal{I}_{\mathbf{U}_{0,\mathcal{D}}} : \mathcal{C}_0^0(\overline{\Omega}\backslash\Gamma)^d \to \mathbf{U}_{0,\mathcal{D}}$ is defined through its components by setting, for $\mathbf{v} \in \mathcal{C}_0^0(\overline{\Omega}\backslash\Gamma)^d$,

$$(\mathcal{I}_{\mathbf{U}_{0,\mathcal{D}}} \mathbf{v})_{\mathcal{K}s} = \mathbf{v}_{|K}(\mathbf{x}_s) \quad \forall K \in \mathcal{M}\,,\ \forall s \in \mathcal{V}_K. \tag{14}$$

We note that, since $\mathbf{v} = 0$ on $\partial\Omega$, this operator indeed defines an element in $\mathbf{U}_{0,\mathcal{D}}$.

3.6 Nitsche's discretisation

The normal surface traction operator on the + side of the fracture network $\boldsymbol{\sigma}_{\mathcal{D},\mathbf{n}} : \mathbf{U}_{0,\mathcal{D}} \to L^2(\Gamma)$ is defined by

$$\sigma_{\mathcal{D},\mathbf{n}}(\mathbf{v}_\mathcal{D})|_\sigma = \gamma_\mathbf{n}^+(\boldsymbol{\sigma}_\mathcal{D}(\mathbf{v}_\mathcal{D})) \cdot \mathbf{n}^+.$$

For a parameter $\theta \in \mathbb{R}$, we define the operator $P_{\mathcal{D},\beta,\theta} : \mathbf{U}_{0,\mathcal{D}} \to L^2(\Gamma)$ by

$$P_{\mathcal{D},\beta,\theta}(\mathbf{v}_\mathcal{D}) = \theta\sigma_{\mathcal{D},\mathbf{n}}(\mathbf{v}_\mathcal{D}) - \beta[\![\mathbf{v}_\mathcal{D}]\!]_{\mathcal{D},\mathbf{n}}$$

and we set $P_{\mathcal{D},\beta} = P_{\mathcal{D},\beta,1}$, with the function $\beta \in \mathbb{P}^0(\mathcal{F}_\Gamma)$ such that

$$\beta|_\sigma = \frac{\beta_0}{h_\sigma} \quad \forall \sigma \in \mathcal{F}_\Gamma,$$

and β_0 the Nitsche's penalisation parameter. We can now introduce the Nitsche's discretisation for addressing the contact-mechanics problem. Find $\mathbf{u}_\mathcal{D} \in \mathbf{U}_{0,\mathcal{D}}$ such that, for all $\mathbf{v}_\mathcal{D} \in \mathbf{U}_{0,\mathcal{D}}$,

$$\begin{aligned} &\int_\Omega \boldsymbol{\sigma}_\mathcal{D}(\mathbf{u}_\mathcal{D}) : \boldsymbol{\epsilon}_\mathcal{D}(\mathbf{v}_\mathcal{D}) + S_{\mu,\lambda,\mathcal{D}}(\mathbf{u}_\mathcal{D}, \mathbf{v}_\mathcal{D}) - \int_\Gamma \frac{\theta}{\beta}\sigma_{\mathcal{D},\mathbf{n}}(\mathbf{u}_\mathcal{D})\sigma_{\mathcal{D},\mathbf{n}}(\mathbf{v}_\mathcal{D}) \\ &+ \int_\Gamma \frac{1}{\beta}[P_{\mathcal{D},\beta}(\mathbf{u}_\mathcal{D})]_{\mathbb{R}^-} P_{\mathcal{D},\beta,\theta}(\mathbf{v}_\mathcal{D}) = \int_\Omega \mathbf{f} \cdot \widetilde{\Pi}^\mathcal{D}\mathbf{v}_\mathcal{D}. \end{aligned} \tag{15}$$

The positive parameter β_0 plays the role of a stabilisation parameter which needs to be large enough in order to ensure the stability and accuracy of the discretisation as shown in the next section. The parameter θ encompasses symmetric and non-symmetric variants of the method [21]. The symmetric case obtained for $\theta = 1$ can be advantageous to use solvers for symmetric matrices, while the choice $\theta = 0$ leads to a simplified variational formulation, easier to extend to large strain. The choice $\theta = -1$ has the remarkable property to provide a stability of the discretisation irrespectively of the value of the stabilisation parameter as shown in the subsequent analysis.

As already noticed in [19], the Nitsche's formulation (15) has closed links with the Barbosa and Hughes stabilised mixed formulation introduced in [37] and extended to contact mechanics in [36]. The difference is that, for the Nitsche's formulation, the Lagrange multiplier accounting for the normal surface traction is taken in $\{\mu \in L^2(\Gamma) \,|\, \mu \geq 0\}$ and can be eliminated from the mixed formulation. For facewise constant Lagrange multipliers, a strict equivalence can be shown using a mean value approximation of the normal surface traction and jump in the Nitsche's terms [3].

4 Numerical analysis

In Section 4.1, we introduce or recall from [29] preliminary definitions and lemmae. Section 4.2 establishes the well-posedness of the scheme (15). Then, Section (4.3) first proves an abstract error estimate which is used to obtain an optimal first order error estimate with minimal regularity assumption on the solution.

4.1 Preliminary definitions and lemmae

Assuming that $\Omega\backslash\overline{\Gamma}$ is connected, the semi-norm given for all $\mathbf{v}_\mathcal{D} \in \mathbf{U}_{0,\mathcal{D}}$

$$\|\mathbf{v}_\mathcal{D}\|_{1,\mathcal{D}} := \left(\|\nabla^\mathcal{D}\mathbf{v}_\mathcal{D}\|^2_{L^2(\Omega\backslash\overline{\Gamma})} + S_\mathcal{D}(\mathbf{v}_\mathcal{D}, \mathbf{v}_\mathcal{D})\right)^{1/2}, \tag{16}$$

defines a H^1-like discrete norm on $\mathbf{U}_{0,\mathcal{D}}$.

Lemma 4.1 (Discrete Poincaré inequality)**.** *There exists $C_{P,\mathcal{D}}$ depending only on Ω, Γ and the mesh regularity such that for all $\mathbf{v}_\mathcal{D} \in \mathbf{U}_{0,\mathcal{D}}$, one has*

$$\|\widetilde{\Pi}^{\mathcal{D}}\mathbf{v}_\mathcal{D}\|_{L^2(\Omega\backslash\overline{\Gamma})} \leq C_{P,\mathcal{D}}\|\mathbf{v}_\mathcal{D}\|_{1,\mathcal{D}}.$$

Proof. Using the discrete Poincaré inequality for the Hybrid Finite Volume discretisation [32], it holds that

$$\|\widetilde{\Pi}^{\mathcal{D}}\mathbf{v}_\mathcal{D}\|^2_{L^2(\Omega\backslash\overline{\Gamma})} = \sum_{K\in\mathcal{M}} |K||\overline{\mathbf{v}}_K|^2 \lesssim \sum_{K\in\mathcal{M}}\sum_{\sigma\in\mathcal{F}_K} h_K|\sigma|\Big(\frac{|\overline{\mathbf{v}}_{K\sigma}-\overline{\mathbf{v}}_K|}{h_K}\Big)^2.$$

Since from Lemma 5.11 of [29], one has

$$\sum_{K\in\mathcal{M}}\sum_{\sigma\in\mathcal{F}_K} h_K|\sigma|\Big(\frac{|\overline{\mathbf{v}}_{K\sigma}-\overline{\mathbf{v}}_K|}{h_K}\Big)^2 \lesssim \|\mathbf{v}_\mathcal{D}\|^2_{1,\mathcal{D}},$$

the result is proved. □

Let us recall the following discrete Korn's inequality already proved in Theorem 5.7 of [29].

Lemma 4.2 (Discrete Korn's inequality)**.** *Assuming that $\Omega\backslash\overline{\Gamma}$ is connected, it holds*

$$\|\mathbf{v}_\mathcal{D}\|^2_{1,\mathcal{D}} \lesssim \|\boldsymbol{\epsilon}_\mathcal{D}(\mathbf{v}_\mathcal{D})\|^2_{L^2(\Omega\backslash\overline{\Gamma})} + S_\mathcal{D}(\mathbf{v}_\mathcal{D},\mathbf{v}_\mathcal{D}) \qquad \forall \mathbf{v}_\mathcal{D}\in\mathbf{U}_{0,\mathcal{D}}, \tag{17}$$

with a constant depending on Ω, Γ and the regularity of the mesh.

To shorten the notations, let us define the discrete energy inner product $\langle .,.\rangle_{e,\mathcal{D}}$ such that, $\forall \mathbf{u}_\mathcal{D},\mathbf{v}_\mathcal{D}\in\mathbf{U}_{0,\mathcal{D}}$

$$\langle \mathbf{u}_\mathcal{D},\mathbf{v}_\mathcal{D}\rangle_{e,\mathcal{D}} = \int_\Omega \boldsymbol{\sigma}_\mathcal{D}(\mathbf{u}_\mathcal{D}) : \boldsymbol{\epsilon}_\mathcal{D}(\mathbf{v}_\mathcal{D}) + S_{\mu,\lambda,\mathcal{D}}(\mathbf{u}_\mathcal{D},\mathbf{v}_\mathcal{D}), \tag{18}$$

and denote by $\|.\|_{e,\mathcal{D}}$ its associated norm. From the above discrete Korn's inequality, we deduce the following bound for all $\mathbf{v}_\mathcal{D}\in\mathbf{U}_{0,\mathcal{D}}$

$$\|\mathbf{v}_\mathcal{D}\|_{1,\mathcal{D}} \lesssim \|\mathbf{v}_\mathcal{D}\|_{e,\mathcal{D}}.$$

We also define $H^{\pm 1/2}$-like discrete norms for all $\mu\in L^2(\Gamma)$ by

$$\|\mu\|_{-1/2,\mathcal{D}} = \Big(\sum_{\sigma\in\mathcal{F}_\Gamma} h_\sigma\|\mu\|^2_{L^2(\sigma)}\Big)^{1/2} \quad\text{and}\quad \|\mu\|_{1/2,\mathcal{D}} = \Big(\sum_{\sigma\in\mathcal{F}_\Gamma} h_\sigma^{-1}\|\mu\|^2_{L^2(\sigma)}\Big)^{1/2}. \tag{19}$$

Lemma 4.3. *There exists $\Lambda_\mathcal{D}$ depending only on Ω, Γ, $\mathbb{A}$, and on the regularity of the mesh such that*

$$\sup_{\mathbf{v}_\mathcal{D}\in\mathbf{U}_{0,\mathcal{D}}:\mathbf{v}_\mathcal{D}\neq 0} \frac{\|\sigma_{\mathcal{D},\mathbf{n}}(\mathbf{v}_\mathcal{D})\|^2_{-1/2,\mathcal{D}}}{\|\mathbf{v}_\mathcal{D}\|^2_{e,\mathcal{D}}} \leq \Lambda_\mathcal{D}.$$

Proof. Let $\mathbf{v}_\mathcal{D}\in\mathbf{U}_\mathcal{D}$, using the uniform ellipticity and boundedness of $\mathbb{A}$ and the mesh regularity, we have

$$\begin{aligned}\|\sigma_{\mathcal{D},\mathbf{n}}(\mathbf{v}_\mathcal{D})\|^2_{-1/2,\mathcal{D}} &= \sum_{\sigma=K|L\in\mathcal{F}_\Gamma} h_\sigma\int_\sigma |(\boldsymbol{\sigma}_\mathcal{D}(\mathbf{v}_\mathcal{D})|_K\mathbf{n}_{K\sigma})\cdot\mathbf{n}_{K\sigma}|^2\\ &\lesssim \sum_{\sigma=K|L\in\mathcal{F}_\Gamma}\int_K \boldsymbol{\sigma}_\mathcal{D}(\mathbf{v}_\mathcal{D}):\boldsymbol{\epsilon}_\mathcal{D}(\mathbf{v}_\mathcal{D}) \lesssim \|\mathbf{v}_\mathcal{D}\|^2_{e,\mathcal{D}},\end{aligned}$$

which provides the estimate. □

Let us introduce the space $\mathbf{W}$ of tensor fluxes defined by

$$\mathbf{W} = \big\{\boldsymbol{\sigma} \in H_{\rm div}(\Omega\backslash\overline{\Gamma}; \mathcal{S}^d(\mathbb{R})), : \gamma_{\mathbf{n}}^+(\boldsymbol{\sigma}) + \gamma_{\mathbf{n}}^-(\boldsymbol{\sigma}) = 0, \\ \gamma_{\mathbf{n}}^+(\boldsymbol{\sigma}) \times \mathbf{n}^+ = \mathbf{0},\, \gamma_{\mathbf{n}}^+(\boldsymbol{\sigma}) \cdot \mathbf{n}^+ \in L^2(\Gamma)\big\},$$

where $\mathcal{S}^d(\mathbb{R})$ is the space of symmetric $d \times d$ matrices with real coefficients. The space $\mathbf{W}$ is equipped with the Hilbertian norm

$$\|\boldsymbol{\sigma}\|_{\mathbf{W}} = \Big(\|\boldsymbol{\sigma}\|^2_{L^2(\Omega\backslash\overline{\Gamma})^{d\times d}} + \|\mathbf{div}\boldsymbol{\sigma}\|^2_{L^2(\Omega\backslash\overline{\Gamma})^d} + \|\gamma_{\mathbf{n}}^+(\boldsymbol{\sigma}) \cdot \mathbf{n}^+\|^2_{L^2(\Gamma)}\Big)^{1/2}.$$

Let us define the bilinear form $w_{\mathcal{D}} : \mathbf{W} \times \mathbf{U}_{0,\mathcal{D}} \to \mathbb{R}$ by, $\forall \boldsymbol{\sigma} \in \mathbf{W}, \mathbf{v}_{\mathcal{D}} \in \mathbf{U}_{0,\mathcal{D}}$

$$w_{\mathcal{D}}(\boldsymbol{\sigma}, \mathbf{v}_{\mathcal{D}}) = -\int_\Omega \boldsymbol{\sigma} : \boldsymbol{\epsilon}_{\mathcal{D}}(\mathbf{v}_{\mathcal{D}}) + \int_\Gamma (\gamma_{\mathbf{n}}^+(\boldsymbol{\sigma}) \cdot \mathbf{n}^+)[\![\mathbf{v}_{\mathcal{D}}]\!]_{\mathcal{D},\mathbf{n}} - \int_\Omega \widetilde{\Pi}^{\mathcal{D}}\mathbf{v}_{\mathcal{D}} \cdot \mathbf{div}\boldsymbol{\sigma}. \tag{20}$$

The following adjoint consistency property of the discretisation is proved in Lemma 5.10 of [29].

Lemma 4.4 (Adjoint Consistency)**.** *Let $\mathcal{W}_{\mathcal{D}} : \mathbf{W} \to \mathbb{R}$ be defined as follows: for all $\boldsymbol{\sigma} \in \mathbf{W}$,*

$$\mathcal{W}_{\mathcal{D}}(\boldsymbol{\sigma}) = \sup_{\mathbf{v}_{\mathcal{D}} \in \mathbf{U}_{0,\mathcal{D}}} \frac{w_{\mathcal{D}}(\boldsymbol{\sigma}, \mathbf{v}_{\mathcal{D}})}{\|\mathbf{v}_{\mathcal{D}}\|_{1,\mathcal{D}}},$$

then, for all $\boldsymbol{\sigma} \in \mathbf{W}$ such that $\boldsymbol{\sigma}|_K \in H^1(\mathcal{M})^{d\times d}$, we have the estimate

$$\mathcal{W}_{\mathcal{D}}(\boldsymbol{\sigma}) \lesssim h_{\mathcal{D}}|\boldsymbol{\sigma}|_{H^1(\mathcal{M})}. \tag{21}$$

For $\mathbf{u} \in \mathbf{U}_0$ and $\mathbf{v}_{\mathcal{D}} \in \mathbf{U}_{0,\mathcal{D}}$, let us introduce the primal consistency term defined by

$$C_{\mathcal{D}}(\mathbf{u}, \mathbf{v}_{\mathcal{D}}) = \Big(\|\nabla\mathbf{u} - \nabla^{\mathcal{D}}\mathbf{v}_{\mathcal{D}}\|^2_{L^2(\Omega\backslash\overline{\Gamma})} + S_{\mathcal{D}}(\mathbf{v}_{\mathcal{D}}, \mathbf{v}_{\mathcal{D}})\Big)^{1/2}. \tag{22}$$

4.2 Well-posedness

Proposition 4.5. *Let β_0 be such that $\beta_0 > \frac{1}{2}(1+\theta)^2\Lambda_{\mathcal{D}}$, then there exists a unique solution $\mathbf{u}_{\mathcal{D}} \in \mathbf{U}_{0,\mathcal{D}}$ to (15). Moreover it satisfies the following a priori estimate:*

$$\|\mathbf{u}_{\mathcal{D}}\|_{1,\mathcal{D}} \lesssim \|\mathbf{f}\|_{L^2(\Omega\backslash\overline{\Gamma})},$$

with a constant depending only on Ω, Γ, $\mathbb{A}$, and the regularity of the mesh but independent on β_0 and θ.

Proof. The proof proposed in [21] in the conforming Finite Element case is readily adapted to our non-conforming framework. Let us define the operator $B_{\mathcal{D}} : \mathbf{U}_{0,\mathcal{D}} \to \mathbf{U}_{0,\mathcal{D}}$ such that

$$\langle B_{\mathcal{D}}\mathbf{v}_{\mathcal{D}}, \mathbf{w}_{\mathcal{D}}\rangle_{e,\mathcal{D}} = \langle \mathbf{v}_{\mathcal{D}}, \mathbf{w}_{\mathcal{D}}\rangle_{e,\mathcal{D}} - \int_\Gamma \frac{\theta}{\beta}\sigma_{\mathcal{D},\mathbf{n}}(\mathbf{v}_{\mathcal{D}})\sigma_{\mathcal{D},\mathbf{n}}(\mathbf{w}_{\mathcal{D}}) \\ + \int_\Gamma \frac{1}{\beta}[P_{\mathcal{D},\beta}(\mathbf{v}_{\mathcal{D}})]_{\mathbb{R}^-} P_{\mathcal{D},\beta,\theta}(\mathbf{w}_{\mathcal{D}})$$

for all $\mathbf{v}_\mathcal{D}, \mathbf{w}_\mathcal{D} \in \mathbf{U}_{0,\mathcal{D}}$. Writing $P_{\mathcal{D},\beta,\theta}(\mathbf{u}_\mathcal{D} - \mathbf{v}_\mathcal{D}) = P_{\mathcal{D},\beta}(\mathbf{u}_\mathcal{D} - \mathbf{v}_\mathcal{D}) + (\theta-1)\sigma_{\mathcal{D},\mathbf{n}}(\mathbf{u}_\mathcal{D} - \mathbf{v}_\mathcal{D})$, using $([a]_{\mathbb{R}^-} - [b]_{\mathbb{R}^-})(a-b) \geq ([a]_{\mathbb{R}^-} - [b]_{\mathbb{R}^-})^2$ for all $a, b \in \mathbb{R}$, Cauchy-Schwarz and Young's inequalities, we have for all $c > 0$

$$\begin{aligned}\langle B_\mathcal{D}\mathbf{u}_\mathcal{D} - B_\mathcal{D}\mathbf{v}_\mathcal{D}, \mathbf{u}_\mathcal{D} - \mathbf{v}_\mathcal{D}\rangle_{e,\mathcal{D}} \geq \|\mathbf{u}_\mathcal{D} - \mathbf{v}_\mathcal{D}\|_{e,\mathcal{D}}^2 - \frac{\theta}{\beta_0}\|\sigma_{\mathcal{D},\mathbf{n}}(\mathbf{u}_\mathcal{D} - \mathbf{v}_\mathcal{D})\|_{-1/2,\mathcal{D}}^2 \\ + \frac{1}{\beta_0}\|[P_{\mathcal{D},\beta}(\mathbf{u}_\mathcal{D})]_{\mathbb{R}^-} - [P_{\mathcal{D},\beta}(\mathbf{v}_\mathcal{D})]_{\mathbb{R}^-}\|_{-1/2,\mathcal{D}}^2 \\ - \frac{1}{\beta_0}\frac{|\theta-1|}{2c}\|[P_{\mathcal{D},\beta}(\mathbf{u}_\mathcal{D})]_{\mathbb{R}^-} - [P_{\mathcal{D},\beta}(\mathbf{v}_\mathcal{D})]_{\mathbb{R}^-}\|_{-1/2,\mathcal{D}}^2 \\ - \frac{1}{\beta_0}\frac{|\theta-1|c}{2}\|\sigma_{\mathcal{D},\mathbf{n}}(\mathbf{u}_\mathcal{D} - \mathbf{v}_\mathcal{D}\|_{-1/2,\mathcal{D}}^2.\end{aligned}$$

Choosing $c = \frac{|\theta-1|}{2}$ and using Lemma 4.3 we obtain the estimate

$$\langle B_\mathcal{D}\mathbf{u}_\mathcal{D} - B_\mathcal{D}\mathbf{v}_\mathcal{D}, \mathbf{u}_\mathcal{D} - \mathbf{v}_\mathcal{D}\rangle_{e,\mathcal{D}} \geq \Big(1 - \frac{(1+\theta)^2}{4\beta_0}\Lambda_\mathcal{D}\Big)\|\mathbf{u}_\mathcal{D} - \mathbf{v}_\mathcal{D}\|_{e,\mathcal{D}}^2, \tag{23}$$

which shows that $B_\mathcal{D}$ is an M-operator as soon as $\beta_0 > \frac{1}{4}(1+\theta)^2\Lambda_\mathcal{D}$. Using that $|[a]_{\mathbb{R}^-} - [b]_{\mathbb{R}^-}| \leq |a-b|$ for all $a, b \in \mathbb{R}$, it can also be shown as in [21] that $B_\mathcal{D}$ is an hemicontinuous operator in the sense that the function $t \to \langle B_\mathcal{D}(\mathbf{u}_\mathcal{D} - t\mathbf{w}_\mathcal{D}), \mathbf{w}_\mathcal{D}\rangle_{e,\mathcal{D}}$ is a continuous real function for all $\mathbf{v}_\mathcal{D}, \mathbf{w}_\mathcal{D} \in \mathbf{U}_{0,\mathcal{D}}$. From its M-operator property and hemicontinuity, applying Corollary 15 (p. 126) of [14], it results that $B_\mathcal{D}$ is a one to one operator from which the existence and uniqueness of $\mathbf{u}_\mathcal{D}$ is deduced. The estimate on $\mathbf{u}_\mathcal{D}$ is derived from $\langle B_\mathcal{D}\mathbf{u}_\mathcal{D}, \mathbf{u}_\mathcal{D}\rangle_{e,\mathcal{D}} = \int_\Omega \mathbf{f}\cdot\widetilde{\Pi}^D\mathbf{u}_\mathcal{D}$, the discrete Poincaré inequality of Lemma 4.1 and Korn's inequality of Lemma 4.2. □

4.3 Error estimate

Let us first derive the following abstract error estimate.

Theorem 4.6. *Let* $\mathbf{u}$ *the solution of* (3) *with* $\sigma_\mathbf{n}(\mathbf{u}) \in L^2(\Gamma)$, *and* $\mathbf{u}_\mathcal{D}$ *the solution of* (15). *Then, for* $\beta_0 \geq 4(\theta + \frac{|\theta|}{2} + |1-\theta|^2)\Lambda_\mathcal{D}$ *we have the estimate*

$$\begin{aligned}\|\nabla\mathbf{u} - \nabla^\mathcal{D}\mathbf{u}_\mathcal{D}\|_{L^2(\Omega\setminus\overline{\Gamma})} + \frac{1}{\beta_0}\|\sigma_\mathbf{n}(\mathbf{u}) - [P_{\mathcal{D},\beta}(\mathbf{u}_\mathcal{D})]_{\mathbb{R}^-}\|_{-1/2,\mathcal{D}} \\ \lesssim \mathcal{W}_\mathcal{D}(\boldsymbol{\sigma}(\mathbf{u})) + \inf_{\mathbf{v}_\mathcal{D}\in\mathbf{U}_{0,\mathcal{D}}}\Big\{C_\mathcal{D}(\mathbf{u}, \mathbf{v}_\mathcal{D}) + \frac{1}{\beta_0}\|\sigma_\mathbf{n}(\mathbf{u}) - \sigma_{\mathcal{D},\mathbf{n}}(\mathbf{v}_\mathcal{D})\|_{-1/2,\mathcal{D}} \\ + \beta_0\|[\![\mathbf{u}]\!]_\mathbf{n} - [\![\mathbf{v}_\mathcal{D}]\!]_{\mathcal{D},\mathbf{n}}\|_{1/2,\mathcal{D}}\Big\},\end{aligned} \tag{24}$$

with a constant depending only on Ω, Γ, $\mathbb{A}$, θ *and the regularity of the mesh. Moreover, for* $\theta = -1$, *the estimate holds for* $\beta_0 > 0$ *at the expense of a constant depending additionnally on* β_0.

Proof. From (4), we have for all $\mathbf{w}_\mathcal{D} \in \mathbf{U}_{0,\mathcal{D}}$ that

$$-\int_\Gamma \sigma_{\mathcal{D},\mathbf{n}}(\mathbf{u})[\![\mathbf{w}_\mathcal{D}]\!]_{\mathcal{D},\mathbf{n}} = -\int_\Gamma \frac{\theta}{\beta}\sigma_\mathbf{n}(\mathbf{u})\sigma_{\mathcal{D},\mathbf{n}}(\mathbf{w}_\mathcal{D}) + \int_\Gamma \frac{1}{\beta}[P_\beta(\mathbf{u})]_{\mathbb{R}^-}P_{\mathcal{D},\beta,\theta}(\mathbf{w}_\mathcal{D}). \tag{25}$$

Combining (25) with the adjoint consistency (20) for $\boldsymbol{\sigma} = \boldsymbol{\sigma}(\mathbf{u})$ with $\mathbf{div}\boldsymbol{\sigma} = -\mathbf{f}$, $(\gamma_{\mathbf{n}}^{+}\boldsymbol{\sigma}) \cdot \mathbf{n}^{+} = \sigma_{\mathbf{n}}(\mathbf{u})$, we have

$$\begin{aligned}&\int_{\Omega} \boldsymbol{\sigma}(\mathbf{u}) : \boldsymbol{\epsilon}_{\mathcal{D}}(\mathbf{w}_{\mathcal{D}}) - \int_{\Gamma} \frac{\theta}{\beta}\sigma_{\mathbf{n}}(\mathbf{u})\sigma_{\mathcal{D},\mathbf{n}}(\mathbf{w}_{\mathcal{D}}) + \int_{\Gamma} \frac{1}{\beta}[P_{\beta}(\mathbf{u})]_{\mathbb{R}^-} P_{\mathcal{D},\beta,\theta}(\mathbf{w}_{\mathcal{D}}) \\ &- \int_{\Omega} \mathbf{f} \cdot \widetilde{\Pi}^{\mathcal{D}}\mathbf{w}_{\mathcal{D}} = -w_{\mathcal{D}}(\boldsymbol{\sigma}(\mathbf{u}), \mathbf{w}_{\mathcal{D}}).\end{aligned} \tag{26}$$

Combining (26) with the scheme (15) we get

$$\begin{aligned}&\int_{\Omega} (\boldsymbol{\sigma}_{\mathcal{D}}(\mathbf{u}_{\mathcal{D}}) - \boldsymbol{\sigma}(\mathbf{u})) : \boldsymbol{\epsilon}_{\mathcal{D}}(\mathbf{w}_{\mathcal{D}}) + S_{\mu,\lambda,\mathcal{D}}(\mathbf{u}_{\mathcal{D}}, \mathbf{w}_{\mathcal{D}}) - w_{\mathcal{D}}(\boldsymbol{\sigma}(\mathbf{u}), \mathbf{w}_{\mathcal{D}}) \\ &= \int_{\Gamma} \frac{\theta}{\beta}(\sigma_{\mathcal{D},\mathbf{n}}(\mathbf{u}_{\mathcal{D}}) - \sigma_{\mathbf{n}}(\mathbf{u}))\sigma_{\mathcal{D},\mathbf{n}}(\mathbf{w}_{\mathcal{D}}) \\ &\quad - \int_{\Gamma} \frac{1}{\beta}\Big([P_{\mathcal{D},\beta}(\mathbf{u}_{\mathcal{D}})]_{\mathbb{R}^-} - [P_{\beta}(\mathbf{u})]_{\mathbb{R}^-}\Big) P_{\mathcal{D},\beta,\theta}(\mathbf{w}_{\mathcal{D}}).\end{aligned} \tag{27}$$

Setting $\mathbf{w}_{\mathcal{D}} = \mathbf{u}_{\mathcal{D}} - \mathbf{v}_{\mathcal{D}}$ for $\mathbf{v}_{\mathcal{D}} \in \mathbf{U}_{0,\mathcal{D}}$ we obtain

$$\begin{aligned}\|\mathbf{u}_{\mathcal{D}} - \mathbf{v}_{\mathcal{D}}\|_{e,\mathcal{D}}^2 = &\int_{\Omega} (\boldsymbol{\sigma}(\mathbf{u}) - \boldsymbol{\sigma}_{\mathcal{D}}(\mathbf{v}_{\mathcal{D}})) : \boldsymbol{\epsilon}_{\mathcal{D}}(\mathbf{u}_{\mathcal{D}} - \mathbf{v}_{\mathcal{D}}) - S_{\mu,\lambda,\mathcal{D}}(\mathbf{v}_{\mathcal{D}}, \mathbf{u}_{\mathcal{D}} - \mathbf{v}_{\mathcal{D}}) \\ &+ w_{\mathcal{D}}(\boldsymbol{\sigma}(\mathbf{u}), \mathbf{u}_{\mathcal{D}} - \mathbf{v}_{\mathcal{D}}) + A_1 + A_2,\end{aligned} \tag{28}$$

with

$$A_1 = \int_{\Gamma} \frac{\theta}{\beta}(\sigma_{\mathcal{D},\mathbf{n}}(\mathbf{u}_{\mathcal{D}}) - \sigma_{\mathbf{n}}(\mathbf{u}))\sigma_{\mathcal{D},\mathbf{n}}(\mathbf{u}_{\mathcal{D}} - \mathbf{v}_{\mathcal{D}}),$$

and

$$A_2 = -\int_{\Gamma} \frac{1}{\beta}\Big([P_{\mathcal{D},\beta}(\mathbf{u}_{\mathcal{D}})]_{\mathbb{R}^-} - [P_{\beta}(\mathbf{u})]_{\mathbb{R}^-}\Big) P_{\mathcal{D},\beta,\theta}(\mathbf{u}_{\mathcal{D}} - \mathbf{v}_{\mathcal{D}}).$$

First, using Cauchy-Schwarz, Young and the discrete Korn (17) inequalities, we obtain that there exists a constant c_0 such that

$$\begin{aligned}&\int_{\Omega} (\boldsymbol{\sigma}(\mathbf{u}) - \boldsymbol{\sigma}_{\mathcal{D}}(\mathbf{v}_{\mathcal{D}})) : \boldsymbol{\epsilon}_{\mathcal{D}}(\mathbf{u}_{\mathcal{D}} - \mathbf{v}_{\mathcal{D}}) - S_{\mu,\lambda,\mathcal{D}}(\mathbf{v}_{\mathcal{D}}, \mathbf{u}_{\mathcal{D}} - \mathbf{v}_{\mathcal{D}}) + w_{\mathcal{D}}(\boldsymbol{\sigma}(\mathbf{u}), \mathbf{u}_{\mathcal{D}} - \mathbf{v}_{\mathcal{D}}) \\ &\leq \frac{1}{2}\|\mathbf{u}_{\mathcal{D}} - \mathbf{v}_{\mathcal{D}}\|_{e,\mathcal{D}}^2 + c_0\Big(C_D(\mathbf{u}, \mathbf{v}_{\mathcal{D}})^2 + \mathcal{W}_{\mathcal{D}}(\boldsymbol{\sigma}(\mathbf{u}))^2\Big).\end{aligned} \tag{29}$$

The contact terms A_1 and A_2 are estimated as in [21]. Starting with A_1, writing

$$\sigma_{\mathcal{D},\mathbf{n}}(\mathbf{u}_{\mathcal{D}}) - \sigma_{\mathbf{n}}(\mathbf{u}) = \sigma_{\mathcal{D},\mathbf{n}}(\mathbf{u}_{\mathcal{D}} - \mathbf{v}_{\mathcal{D}}) + \sigma_{\mathcal{D},\mathbf{n}}(\mathbf{v}_{\mathcal{D}}) - \sigma_{\mathbf{n}}(\mathbf{u}),$$

and using Cauchy-Schwarz and Young's inequalities and Lemma 4.3, we obtain that for all $c_1 > 0$:

$$\begin{aligned}\beta_0 A_1 &\leq (\theta + \frac{|\theta|}{2c_1})\|\sigma_{\mathcal{D},\mathbf{n}}(\mathbf{u}_{\mathcal{D}} - \mathbf{v}_{\mathcal{D}})\|_{-1/2,\mathcal{D}}^2 + \frac{c_1|\theta|}{2}\|\sigma_{\mathbf{n}}(\mathbf{u}) - \sigma_{\mathcal{D},\mathbf{n}}(\mathbf{v}_{\mathcal{D}})\|_{-1/2,\mathcal{D}}^2 \\ &\leq (\theta + \frac{|\theta|}{2c_1})\Lambda_{\mathcal{D}}\|\mathbf{u}_{\mathcal{D}} - \mathbf{v}_{\mathcal{D}}\|_{e,\mathcal{D}}^2 + \frac{c_1|\theta|}{2}\|\sigma_{\mathbf{n}}(\mathbf{u}) - \sigma_{\mathcal{D},\mathbf{n}}(\mathbf{v}_{\mathcal{D}})\|_{-1/2,\mathcal{D}}^2\end{aligned} \tag{30}$$

Writing

$$\begin{aligned}P_{\mathcal{D},\beta,\theta}(\mathbf{u}_{\mathcal{D}} - \mathbf{v}_{\mathcal{D}}) =&P_{\mathcal{D},\beta}(\mathbf{u}_{\mathcal{D}} - \mathbf{v}_{\mathcal{D}}) + (\theta - 1)\sigma_{\mathcal{D},\mathbf{n}}(\mathbf{u}_{\mathcal{D}} - \mathbf{v}_{\mathcal{D}}) \\ =&(P_{\mathcal{D},\beta}(\mathbf{u}_{\mathcal{D}}) - P_{\beta}(\mathbf{u})) + (\sigma_{\mathbf{n}}(\mathbf{u}) - \sigma_{\mathcal{D},\mathbf{n}}(\mathbf{v}_{\mathcal{D}})) - \beta([\![\mathbf{u}]\!]_{\mathbf{n}} - [\![\mathbf{v}_{\mathcal{D}}]\!]_{\mathcal{D},\mathbf{n}}) \\ &+ (\theta - 1)\sigma_{\mathcal{D},\mathbf{n}}(\mathbf{u}_{\mathcal{D}} - \mathbf{v}_{\mathcal{D}}),\end{aligned}$$

and using that $([a]_{\mathbb{R}^-} - [b]_{\mathbb{R}^-})(a-b) \geq ([a]_{\mathbb{R}^-} - [b]_{\mathbb{R}^-})^2$ for all $a, b \in \mathbb{R}$, Cauchy-Schwarz and Young's inequalities, and Lemma 4.3, we obtain that for all $c_2 > 0$, $c_3 > 0$:

$$\begin{aligned}\beta_0 A_2 \leq & \Big(-1 + \frac{1}{2c_2} + \frac{|1-\theta|}{2c_3}\Big) \|[P_{\mathcal{D},\beta}(\mathbf{u}_\mathcal{D})]_{\mathbb{R}^-} - [P_\beta(\mathbf{u})]_{\mathbb{R}^-}\|^2_{-1/2,\mathcal{D}} \\ & + c_2 \Big(\|\sigma_\mathbf{n}(\mathbf{u}) - \sigma_{\mathcal{D},\mathbf{n}}(\mathbf{v}_\mathcal{D})\|^2_{-1/2,\mathcal{D}} + \beta_0^2 \|[\![\mathbf{u}]\!]_\mathbf{n} - [\![\mathbf{v}_\mathcal{D}]\!]_{\mathcal{D},\mathbf{n}}\|^2_{1/2,\mathcal{D}} \Big) \\ & + \frac{|1-\theta| c_3}{2} \Lambda_\mathcal{D} \|\mathbf{u}_\mathcal{D} - \mathbf{v}_\mathcal{D}\|^2_{e,\mathcal{D}}.\end{aligned} \tag{31}$$

Gathering (29)-(30)-(31) in (28) and using $\sigma_\mathbf{n}(\mathbf{u}) = [P_\beta(\mathbf{u})]_{\mathbb{R}^-}$, we obtain the estimate

$$\begin{aligned}\frac{1}{2}\|\mathbf{u}_\mathcal{D} - \mathbf{v}_\mathcal{D}\|^2_{e,\mathcal{D}} \leq & \frac{1}{\beta_0}\Big(-1 + \frac{1}{2c_2} + \frac{|1-\theta|}{2c_3}\Big) \|\sigma_\mathbf{n}(\mathbf{u}) - [P_{\mathcal{D},\beta}(\mathbf{u}_\mathcal{D})]_{\mathbb{R}^-}\|^2_{-1/2,\mathcal{D}} \\ & + \frac{1}{\beta_0}\Big(\theta + \frac{|\theta|}{2c_1} + \frac{|1-\theta|c_3}{2}\Big) \Lambda_\mathcal{D} \|\mathbf{u}_\mathcal{D} - \mathbf{v}_\mathcal{D}\|^2_{e,\mathcal{D}} \\ & + c_0 \Big(C_D(\mathbf{u}, \mathbf{v}_\mathcal{D})^2 + \mathcal{W}_\mathcal{D}(\boldsymbol{\sigma}(\mathbf{u}))^2 \Big) \\ & + \frac{1}{\beta_0}\Big(c_2 + \frac{c_1|\theta|}{2}\Big) \|\sigma_\mathbf{n}(\mathbf{u}) - \sigma_{\mathcal{D},\mathbf{n}}(\mathbf{v}_\mathcal{D})\|^2_{-1/2,\mathcal{D}} \\ & + \beta_0 c_2 \|[\![\mathbf{u}]\!]_\mathbf{n} - [\![\mathbf{v}_\mathcal{D}]\!]_{\mathcal{D},\mathbf{n}}\|^2_{1/2,\mathcal{D}}.\end{aligned} \tag{32}$$

Choosing $c_1 = 1$, $c_2 = 2$, $c_3 = 2|1-\theta|$, and $\beta_0 \geq 4(\theta + \frac{|\theta|}{2} + |1-\theta|^2)\Lambda_\mathcal{D}$, we obtain

$$\begin{aligned}& \|\mathbf{u}_\mathcal{D} - \mathbf{v}_\mathcal{D}\|^2_{e,\mathcal{D}} + \frac{1}{\beta_0}\|\sigma_\mathbf{n}(\mathbf{u}) - [P_{\mathcal{D},\beta}(\mathbf{u}_\mathcal{D})]_{\mathbb{R}^-}\|^2_{-1/2,\mathcal{D}} \\ & \qquad \lesssim C_D(\mathbf{u}, \mathbf{v}_\mathcal{D})^2 + \mathcal{W}_\mathcal{D}(\boldsymbol{\sigma}(\mathbf{u}))^2 \\ & \qquad\quad + \frac{1}{\beta_0}\|\sigma_\mathbf{n}(\mathbf{u}) - \sigma_{\mathcal{D},\mathbf{n}}(\mathbf{v}_\mathcal{D})\|^2_{-1/2,\mathcal{D}} + \beta_0 \|[\![\mathbf{u}]\!]_\mathbf{n} - [\![\mathbf{v}_\mathcal{D}]\!]_{\mathcal{D},\mathbf{n}}\|^2_{1/2,\mathcal{D}},\end{aligned} \tag{33}$$

with a constant independent on $\mathbf{u}$ and β_0 and depending only on Ω, Γ, $\mathbb{A}$, θ and the mesh regularity. Using the discrete Korn's inequality, this proves (24). For $\theta = -1$, it can be shown as in [21] that c_1, c_2 and c_3 can be chosen in such a way that whatever $\beta_0 > 0$ we have $-1 + \frac{1}{2c_2} + \frac{1}{c_3} < 0$ and $\frac{\Lambda_\mathcal{D}}{\beta_0}(-1 + \frac{1}{2c_1} + c_3) \leq 1/4$ by setting $c_1 = \frac{1}{2\eta}$, $c_2 = 1 + \frac{1}{\eta}$ and $c_3 = 1 + \eta$ and $\eta = \frac{\beta_0}{8\Lambda_\mathcal{D}}$. On the other hand, the constant in (33) depends additionnally on β_0. □

Theorem 4.7. *Let* $\mathbf{u}$ *the solution of* (3) *with* $\mathbf{u} \in H^2(\mathcal{M})^d \cap \mathbf{U}^0$, *and* $\mathbf{u}_\mathcal{D}$ *the solution of* (15). *Then, for* $\beta_0 \geq 4(\theta + \frac{|\theta|}{2} + |1-\theta|^2)\Lambda_\mathcal{D}$ *we have the error estimate*

$$\|\nabla \mathbf{u} - \nabla^\mathcal{D} \mathbf{u}_\mathcal{D}\|_{L^2(\Omega\setminus\overline{\Gamma})} + \frac{1}{\beta_0}\|\sigma_\mathbf{n}(\mathbf{u}) - [P_{\mathcal{D},\beta}(\mathbf{u}_\mathcal{D})]_{\mathbb{R}^-}\|_{-1/2,\mathcal{D}} \lesssim h_\mathcal{D} |\mathbf{u}|_{H^2(\mathcal{M})}, \tag{34}$$

with a constant depending only on Ω, Γ, $\mathbb{A}$, θ *and the regularity of the mesh. Moreover, for* $\theta = -1$, *the estimate holds for* $\beta_0 > 0$ *with a constant depending additionnally on* β_0.

Proof. We set $\mathbf{v}_\mathcal{D} = \mathcal{I}_{\mathbf{U}_{0,\mathcal{D}}} \mathbf{u}$ in (24). Lemma 5.8 of [29] provides the estimate of the gradient reconstruction consistency term

$$C_\mathcal{D}(\mathbf{u}, \mathcal{I}_{\mathbf{U}_{0,\mathcal{D}}} \mathbf{u}) \lesssim h_\mathcal{D} |\mathbf{u}|_{H^2(\mathcal{M})}. \tag{35}$$

From (21), the estimate of the adjoint consistency term is given by

$$\mathcal{W}(\boldsymbol{\sigma}(\mathbf{u})) \lesssim h_\mathcal{D} |\mathbf{u}|_{H^2(\mathcal{M})}. \tag{36}$$

Gathering the estimates (35)-(36), and the estimates (37), (41) of respectively Lemmae 4.8 and 4.9 stated below, concludes the proof. □

Lemma 4.8 (Consistency of the jump reconstruction). *If* $\mathbf{u} \in H^2(\mathcal{M})^d$ *then*

$$\|[\![\mathcal{I}_{\mathbf{U}_{0,\mathcal{D}}}\mathbf{u}]\!]_{\mathcal{D},\mathbf{n}} - [\![\mathbf{u}]\!]_{\mathbf{n}}\|_{1/2,\mathcal{D}} \lesssim h_{\mathcal{D}}|\mathbf{u}|_{H^2(\mathcal{M})}. \tag{37}$$

Proof. From the definition (19) of the $H^{1/2}$-like discrete norm and the definition (8) of the normal jump reconstruction operator, it suffices to prove (considering the + side to fix ideas) that for all $\sigma = K|L \in \mathcal{F}_\Gamma$, one has

$$h_\sigma^{-1/2}\|\Pi^{K\sigma}\mathcal{I}_{\mathbf{U}_{0,\mathcal{D}}}\mathbf{u} - \gamma_+\mathbf{u}\|_{L^2(\sigma)} \lesssim h_K|\mathbf{u}|_{H^2(K)}.$$

Let $\mathbf{q}$ be the $L^2(K)$-orthogonal projection of $\mathbf{u}$ on $\mathbb{P}^1(K)^d$. By the approximation properties of the polynomial projector [26, Theorem 1.45], we have

$$|\mathbf{u} - \mathbf{q}|_{H^s(K)} \lesssim h_K^{2-s}|\mathbf{u}|_{H^2(K)}, \quad \forall s \in \{0,1,2\}. \tag{38}$$

Applying the bound [26, Eq. (5.110)] to $\mathbf{u} - \mathbf{q}$ yields

$$\begin{aligned}\max_K |\mathbf{u} - \mathbf{q}| &\lesssim |K|^{-1/2}\Big(\|\mathbf{u} - \mathbf{q}\|_{L^2(K)} + h_K|\mathbf{u} - \mathbf{q}|_{H^1(K)} + h_K^2|\mathbf{u} - \mathbf{q}|_{H^2(K)}\Big)\\ &\lesssim |K|^{-1/2}h_K^2|\mathbf{u}|_{H^2(K)}.\end{aligned} \tag{39}$$

where the conclusion follows from (38). From the definition (7) of $\Pi^{K\sigma}$ and the mesh regularity it follows that for all $\mathbf{v}_{\mathcal{D}} \in \mathbf{U}_{\mathcal{D}}$ one has

$$\|\Pi^{K\sigma}\mathbf{v}_{\mathcal{D}}\|_{L^\infty(\sigma)} \lesssim \max_{s\in\mathcal{V}_\sigma}|\mathbf{v}_{\mathcal{K}s}|.$$

From the first order polynomial exactness of $\Pi^{K\sigma}$, we deduce that

$$\begin{aligned}\|\Pi^{K\sigma}\mathcal{I}_{\mathbf{U}_{0,\mathcal{D}}}\mathbf{u} - \mathbf{q}\|_{L^\infty(\sigma)} &= \|\Pi^{K\sigma}\mathcal{I}_{\mathbf{U}_{0,\mathcal{D}}}(\mathbf{u} - \mathbf{q})\|_{L^\infty(\sigma)}\\ &\lesssim \|\gamma_+\mathbf{u} - \mathbf{q}\|_{L^\infty(\sigma)}\\ &\lesssim |K|^{-1/2}h_K^2|\mathbf{u}|_{H^2(K)}.\end{aligned}$$

Using this estimate together with (39) and the mesh regularity, we obtain

$$\begin{aligned}h_\sigma^{-1/2}\|\Pi^{K\sigma}\mathcal{I}_{\mathbf{U}_{0,\mathcal{D}}}\mathbf{u} - \gamma_+\mathbf{u}\|_{L^2(\sigma)} &\le h_\sigma^{-1/2}|\sigma|^{1/2}\Big(\|\mathbf{q} - \gamma_+\mathbf{u}\|_{L^\infty(\sigma)}\\ &\qquad + \|\Pi^{K\sigma}\mathcal{I}_{\mathbf{U}_{0,\mathcal{D}}}\mathbf{u} - \mathbf{q}\|_{L^\infty(\sigma)}\Big)\\ &\lesssim h_\sigma^{-1/2}|\sigma|^{1/2}|K|^{-1/2}h_K^2|\mathbf{u}|_{H^2(K)}\\ &\lesssim h_K|\mathbf{u}|_{H^2(K)},\end{aligned} \tag{40}$$

which concludes the proof. □

Lemma 4.9 (Consistency of the normal surface traction reconstruction). *If* $\mathbf{u} \in H^2(\mathcal{M})^d$ *then*

$$\|\sigma_{\mathcal{D},\mathbf{n}}(\mathcal{I}_{\mathbf{U}_{0,\mathcal{D}}}\mathbf{u}) - \sigma_{\mathbf{n}}(\mathbf{u})\|_{-1/2,\mathcal{D}} \lesssim h_{\mathcal{D}}|\mathbf{u}|_{H^2(\mathcal{M})}. \tag{41}$$

Proof. From the uniform boundedness of $\mathbb{A}$, we have

$$\begin{aligned}\|\sigma_{\mathcal{D},\mathbf{n}}(\mathcal{I}_{\mathbf{U}_{0,\mathcal{D}}}\mathbf{u}) - \sigma_{\mathbf{n}}(\mathbf{u})\|_{-1/2,\mathcal{D}} &= \Big(\sum_{\sigma=K|L\in\mathcal{F}_\Gamma} h_\sigma\|\sigma_{\mathbf{n}}(\Pi^K\mathcal{I}_{\mathbf{U}_{0,\mathcal{D}}}\mathbf{u} - \mathbf{u})\|_{L^2(\sigma)}^2\Big)^{1/2}\\ &\lesssim \Big(\sum_{\sigma=K|L\in\mathcal{F}_\Gamma} h_\sigma\|\nabla(\Pi^K\mathcal{I}_{\mathbf{U}_{0,\mathcal{D}}}\mathbf{u} - \mathbf{u})\|_{L^2(\sigma)}^2\Big)^{1/2}.\end{aligned} \tag{42}$$

From the trace inequality given in Lemma 1.31 of [26] (see also [12] and [27]) applied to $\nabla(\Pi^K \mathcal{I}_{\mathbf{U}_{0,\mathcal{D}}}\mathbf{u} - \mathbf{u})$, we obtain that

$$h_K^{1/2}\|\nabla(\Pi^K \mathcal{I}_{\mathbf{U}_{0,\mathcal{D}}}\mathbf{u} - \mathbf{u})\|_{L^2(\sigma)} \lesssim \|\nabla(\Pi^K \mathcal{I}_{\mathbf{U}_{0,\mathcal{D}}}\mathbf{u} - \mathbf{u})\|_{L^2(K)} + h_K|\mathbf{u}|_{H^2(K)}.$$

where we have used the property $|\Pi^K \mathcal{I}_{\mathbf{U}_{0,\mathcal{D}}}\mathbf{u}|_{H^2(K)} = 0$. Combining (42), with this trace inequality and with the gradient consistency error estimate (35), we obtain (41). □

Remark 4.10. Combining the estimate (33) with $\mathbf{v}_\mathcal{D} = \mathcal{I}_{\mathbf{U}_{0,\mathcal{D}}}\mathbf{u}$ together with the estimates in the proof of Theorem 4.7 and the discrete Korn inequality of Lemma 4.2, we obtain the following estimate on the discrete norm $\|\mathbf{u}_\mathcal{D} - \mathcal{I}_{\mathbf{U}_{0,\mathcal{D}}}\mathbf{u}\|_{1,\mathcal{D}}$ which includes the stabilisation term:

$$\|\mathbf{u}_\mathcal{D} - \mathcal{I}_{\mathbf{U}_{0,\mathcal{D}}}\mathbf{u}\|_{1,\mathcal{D}} \lesssim h_\mathcal{D}|\mathbf{u}|_{H^2(\mathcal{M})}. \tag{43}$$

From the previous remark we can derive the following Corollaries.

Corollary 4.11. *Under the same assumptions as in Theorem 4.7, we have the following error estimate on the normal surface traction reconstruction:*

$$\|\sigma_\mathbf{n}(\mathbf{u}) - \sigma_{\mathcal{D},\mathbf{n}}(\mathbf{u}_\mathcal{D})\|_{-1/2,\mathcal{D}} \lesssim h_\mathcal{D}|\mathbf{u}|_{H^2(\mathcal{M})}. \tag{44}$$

Proof. Using Lemma 4.3 for $\mathbf{u}_\mathcal{D} - \mathcal{I}_{\mathbf{U}_{0,\mathcal{D}}}\mathbf{u}$ and the estimate (43), we obtain that

$$\|\sigma_{\mathcal{D},\mathbf{n}}(\mathcal{I}_{\mathbf{U}_{0,\mathcal{D}}}\mathbf{u}) - \sigma_{\mathcal{D},\mathbf{n}}(\mathbf{u}_\mathcal{D})\|_{-1/2,\mathcal{D}} \lesssim h_\mathcal{D}|\mathbf{u}|_{H^2(\mathcal{M})},$$

which, combined with the estimate of Lemma 4.9 concludes the proof. □

The second Corollary states an error estimate for the VEM virtual function reconstruction in $H^1(\Omega\backslash\overline{\Gamma})$ denoted by $\pi_h\mathbf{u}_\mathcal{D}$ (see [6, 5]).

Corollary 4.12. *Under the same assumptions as in Theorem 4.7, we have the following error estimate on the VEM virtual function reconstruction:*

$$\|\nabla\mathbf{u} - \nabla\pi_h\mathbf{u}_\mathcal{D}\|_{L^2(\Omega\backslash\overline{\Gamma})} \lesssim h_\mathcal{D}|\mathbf{u}|_{H^2(\mathcal{M})}. \tag{45}$$

Proof. Using the VEM stability property [6, 5, 4, 13] combined with the estimate (43), we obtain that

$$\|\nabla(\pi_h\mathcal{I}_{\mathbf{U}_{0,\mathcal{D}}}\mathbf{u}) - \nabla\pi_h\mathbf{u}_\mathcal{D}\|_{L^2(\Omega\backslash\overline{\Gamma})} \lesssim \|\mathcal{I}_{\mathbf{U}_{0,\mathcal{D}}}\mathbf{u} - \mathbf{u}_\mathcal{D}\|_{1,\mathcal{D}} \lesssim h_\mathcal{D}|\mathbf{u}|_{H^2(\mathcal{M})}.$$

The proof is concluded from the approximation property of the VEM interpolant $\pi_h\mathcal{I}_{\mathbf{U}_{0,\mathcal{D}}}\mathbf{u}$ stating that $\|\nabla(\pi_h\mathcal{I}_{\mathbf{U}_{0,\mathcal{D}}}\mathbf{u}) - \nabla\mathbf{u}\|_{L^2(\Omega\backslash\overline{\Gamma})} \lesssim h_\mathcal{D}|\mathbf{u}|_{H^2(\mathcal{M})}$ (see [6, 5, 4, 13]). □

5 Numerical experiments

In order to verify numerically the previous error estimate, Section 5.1 studies the convergence of the scheme on various families of meshes based on a 3D manufactured analytical solution with a single fracture. Then, Section 5.2 considers a more complex 3D Discrete Fracture Matrix model using a family of tetrahedral meshes refined along the fracture network, leading to polyhedral meshes. To be more challenging, this test case considers a Coulomb frictional contact model. The VEM Nitsche's discretisation is readily extended to such model and we refer to [39] for a detailed description of this extension. For this test case, the sensitivity

of Nitsche's method to its parameters is investigated, and the scheme is compared with the VEM-bubble discretisation from [28] both in terms of accuracy (using a fine mesh reference solution) and in terms of robustness of the nonlinear solver. The VEM-bubble discretisation uses a mixed formulation with facewise constant Lagrange multipliers combined with a stabilisation based on one bubble displacement additional unknown on one side of each fracture face.

In both cases, the Nitsche's nonlinear term on each fracture face is approximated using a quadrature formula which is exact on second degree polynomials and based on quadrature points defined by the mid edges of a triangular submesh of the given face. The resulting nonlinear system is solved with a semi-smooth Newton algorithm which just amounts to a piecewise differentiation (typically the function $[x]_{\mathbb{R}^-}$ is differenciated according to the sign of $x \in \mathbb{R}$). The stopping criteria is set to 10^{-5} on the relative residual and the linear system at each Newton iteration is solved using the sequential version of the direct sparse solver SuperLU.

5.1 3D manufactured solution

We consider the test case introduced in [28] defined on the domain $\Omega = (-1,1)^3$ with a single non-immersed fracture $\Gamma = \{0\} \times (-1,1)^2$. The material is isotropic and homogeneous given by the Lamé coefficients $\mu = \lambda = 1$. The exact solution

$$\mathbf{u}(x,y,z) = \begin{cases} \begin{pmatrix} g(x,y)p(z) \\ p(z) \\ x^2 p(z) \end{pmatrix} & \text{if } z \geq 0, \\ \begin{pmatrix} h(x)p^+(z) \\ h(x)\left(p^+(z)\right)' \\ -\int_0^x h(\xi)\mathrm{d}\xi \left(p^+(z)\right)' \end{pmatrix} & \text{if } z < 0,\ x\ < 0, \\ \begin{pmatrix} h(x)p^-(z) \\ h(x)\left(p^-(z)\right)' \\ -\int_0^x h(\xi)\mathrm{d}\xi \left(p^-(z)\right)' \end{pmatrix} & \text{if } z < 0,\ x\ \geq 0, \end{cases}$$

with $g(x,y) = -\sin(\frac{\pi x}{2})\cos(\frac{\pi y}{2})$, $p(z) = z^2$, $h(x) = \cos(\frac{\pi x}{2})$, $p^+(z) = z^4$ and $p^-(z) = 2z^4$, is designed to satisfy the frictionless contact conditions at the matrix–fracture interface Γ. The right hand side $\mathbf{f} = -\mathbf{div}\boldsymbol{\sigma}(\mathbf{u})$ and the Dirichlet boundary conditions on $\partial\Omega$ are deduced from $\mathbf{u}$. Note that the fracture Γ is in contact state for $z > 0$ ($[\![\mathbf{u}]\!]_{\mathbf{n}} = 0$) and open for $z < 0$, with a normal jump $[\![\mathbf{u}]\!]_{\mathbf{n}} = -\min(z,0)^4$ depending only on z. The convergence of VEM Nitsche's formulation is investigated on families of uniform Cartesian, tetrahedral and hexahedral meshes. Starting from uniform Cartesian meshes, the hexahedral meshes are generated by random perturbations of the nodes and by cutting non-planar faces into two triangles (see Figure 2). The Nitsche's parameters are fixed to $\theta = -1$ and to $\beta_0 = 100$ (see [3] for more details motivating this choice).

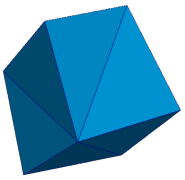

Figure 2: Example of randomly perturbated Cartesian cell with non planar faces cut into two triangles.

Let us define the face-wise constant approximation of the normal surface traction $\lambda = -\sigma_{\mathbf{n}}(\mathbf{u})$ by

$$\lambda_{\mathcal{D}}(\mathbf{x}) = -\Big[\frac{1}{|\sigma|}\int_{\sigma}(|\sigma_{\mathcal{D},\mathbf{n}}(\mathbf{u}_{\mathcal{D}}) - \beta[\![\mathbf{u}_{\mathcal{D}}]\!]_{\mathcal{D},\mathbf{n}})\Big]_{\mathbb{R}^-}, \quad \forall \mathbf{x} \in \sigma, \quad \forall \sigma \in \mathcal{F}_\Gamma, \tag{46}$$

and the reconstruction of the displacement jump vector by

$$[\![\mathbf{u}_{\mathcal{D}}]\!]_{\mathcal{D}}(\mathbf{x}) = \Pi^{K\sigma}\mathbf{u}_{\mathcal{D}}(\mathbf{x}) - \Pi^{L\sigma}\mathbf{u}_{\mathcal{D}}(\mathbf{x}), \quad \forall \mathbf{x} \in \sigma, \quad \forall \sigma = K|L \in \mathcal{F}_\Gamma.$$

Figure 3 exhibits the relative L^2 norms of the errors $\mathbf{u} - \Pi^{\mathcal{D}}\mathbf{u}_{\mathcal{D}}, [\![\mathbf{u}]\!] - [\![\mathbf{u}_{\mathcal{D}}]\!]_{\mathcal{D}}, \nabla\mathbf{u} - \nabla^{\mathcal{D}}\mathbf{u}_{\mathcal{D}}$ and $\lambda - \lambda_{\mathcal{D}}$ on the three family of meshes as a function of the cubic root of the number of cells. It shows, as expected for such a smooth solution, a second-order convergence for $\mathbf{u}$ and $[\![\mathbf{u}]\!]$ with all families of meshes. A first-order convergence is obtained for $\nabla\mathbf{u}$ and λ with both the hexahedral and tetrahedral families of meshes, while a second order super convergence is observed with the family of Cartesian meshes.

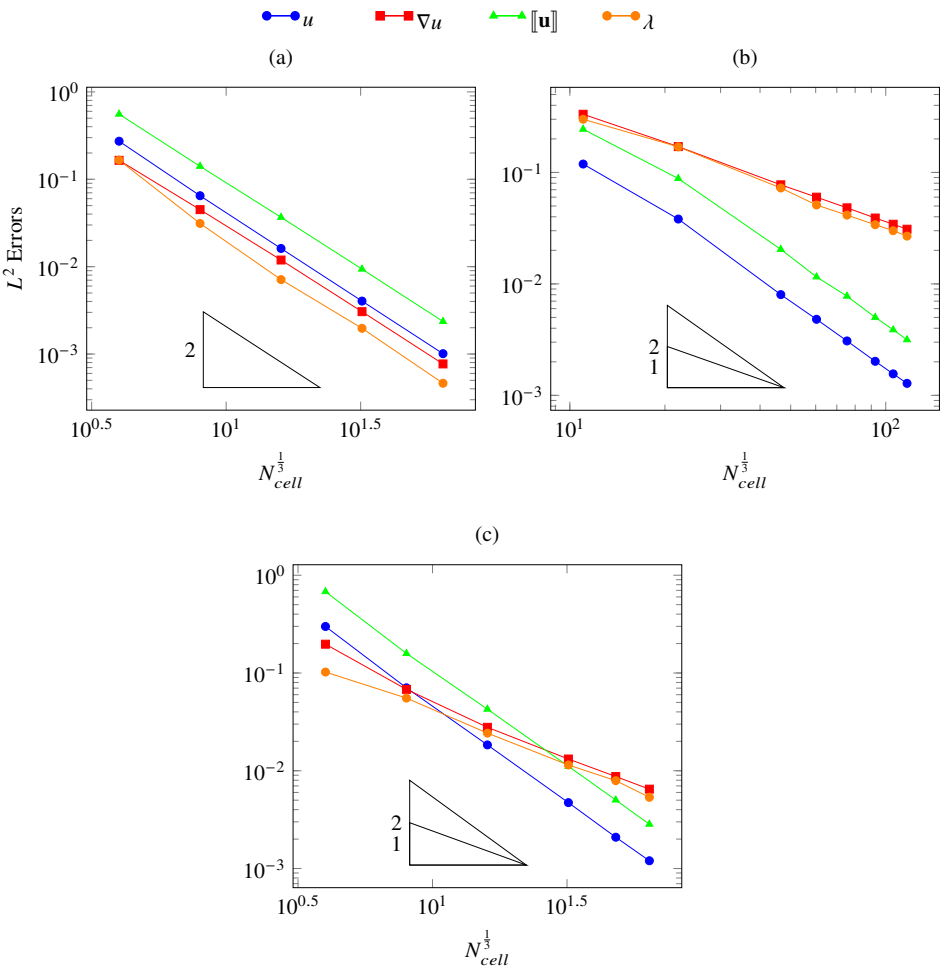

Figure 3: Relative L^2 norms of the errors $\mathbf{u} - \Pi^{\mathcal{D}}\mathbf{u}_{\mathcal{D}}$, $[\![\mathbf{u}]\!] - [\![\mathbf{u}_{\mathcal{D}}]\!]_{\mathcal{D}}$, $\nabla\mathbf{u} - \nabla^{\mathcal{D}}\mathbf{u}_{\mathcal{D}}$ and $\lambda - \lambda_{\mathcal{D}}$ as a function of the cubic root of the number of cells, using the families of Cartesian (a), tetrahedral (b) and hexahedral (c) meshes.

5.2 3D Discrete Fracture Matrix (DFM) model with intersecting fractures

We consider the domain $\Omega = (0, 1, \mathrm{m})^3$ with the fracture network Γ depicted in Figure 4 discretised using tetrahedral meshes containing 47k, 127k, 250k and 450k cells. To improve accuracy, each of these meshes is further refined along the fracture network by cutting each fracture face into 4 triangles leading to conforming polytopal meshes (see the right image in Figure 4). We consider an isotropic homogeneous elastic material with Young's modulus $E = 4\,\mathrm{GPa}$ and Poisson's ratio $\nu = 0.2$ ($\mu = \frac{5}{3}\,\mathrm{GPa}$), combined with a Coulomb frictional contact model with constant friction coefficient $F = 0.75$. Dirichlet boundary conditions are imposed at the bottom and top boundaries for the displacement field with $\mathbf{u} = 0$ at $z = 0$, and $\mathbf{u} = {}^t[0\,\mathrm{m}, 0.005\,\mathrm{m}, -0.002\,\mathrm{m}]$ at $z = 1$. Homogeneous Neumann conditions are imposed at the lateral boundaries. No analytical solution is known for this data set, hence we investigate the numerical convergence of the VEM Nitsche's discretisation using the reference fine mesh solution obtained with 450k cells and the VEM Nitsche's discretisation.

We investigate the sensitivity of Nitsche's discretisation to the normal and tangential penalty parameters β_0^n, β_0^τ (two different values are used in the Coulomb frictional case), and to the parameter θ set typically to either -1, 0, or 1. The well-posedness analysis of

Section 4.2 easily extends to Tresca friction (see e.g. [3] in the FEM case) leading to the sufficient condition $(1+\theta)^2\left(\frac{\Lambda_{\mathcal{D}}}{\beta_0^n}+\frac{\Lambda_{\mathcal{D},\tau}}{\beta_0^\tau}\right)\leq C$, with $C<4$ where Λ_D is defined in Lemma 4.3 and $\Lambda_{\mathcal{D},\tau}$ is defined in the same way based on the tangential traction rather than the normal traction. Using the inverse power algorithm we obtain on the coarsest mesh the following values $\Lambda_{\mathcal{D}}\approx 3.8\mu$ and $\Lambda_{\mathcal{D},\tau}\approx 1.6\mu$ providing an order of magnitude of the penalty parameters. Note that for Coulomb friction additional conditions must be imposed on the penalty parameters to obtain the existence of a discrete solution based on the convergence of a fixed point algorithm related to the Tresca solution [20]. Table 1 investigates, for different values of β_0^n, β_0^τ and θ, the efficiency of the semi-smooth Newton nonlinear solver combined with a backtracking line search algorithm (see [39] for details). As could be expected from the Tresca well-posedness criteria, the choice $\theta=-1$ provides robustness over a larger range of penalty parameters compared with $\theta=0$ or 1. Note however that, at given penalty parameters, the solutions for $\theta=-1,0,1$ exhibit no significant differences for this test case. For small values of the penalty parameters, as could be expected, the solution can exhibit oscillations as illustrated in Figure 5 on the normal displacement jump for $\beta_0^n=5\mu$ and $\beta_0^\tau=2\mu$. Based on these results, we select $\theta=-1$ combined with $\beta_0^n=100\mu$ and $\beta_0^\tau=10\mu$ which offers a good compromise between the accuracy of the solution and the efficiency of the nonlinear solver.

Figure 5 shows no significant differences on the normal displacement jump obtained on the 47k cells mesh with the VEM-bubble discretisation and VEM-Nitsche's method for $\theta=-1$ and $\frac{\beta_0^n}{\mu}=100$ and $\frac{\beta_0^\tau}{\mu}=10$. Figure 6 plots, for both the VEM-Nitsche's and VEM-bubble discretisations, the $\boldsymbol{\tau}_2$-tangential displacement jump along the diagonal of the right vertical fracture obtained on the meshes with 47k, 127k and 250k cells. Here $(\boldsymbol{\tau}_1,\boldsymbol{\tau}_2)$ denotes a local coordinate system on each fracture plane. We observe that Nitsche's method captures more accurately the jump discontinuity at the fracture intersection even on the coarsest meshes while the discontinuity is smoothed out with the VEM-bubble method as a result of the contact conditions satisfied only in average over each fracture face.

Table 2 investigates the numerical behavior of both schemes in terms of number of nonlinear iterations and total CPU time required by each method on the meshes with 47k, 127k, and 250k cells. The results show that VEM-Nitsche's method is more computationally efficient with a similar number of nonlinear iterations for both methods but a lower CPU time for Nitsche's formulation resulting from having half the number of DOFs. This is due to the fact that the VEM-bubble discretisation requires two additional vectorial unknowns (one bubble displacement and one Lagrange multiplier) on each fracture face.

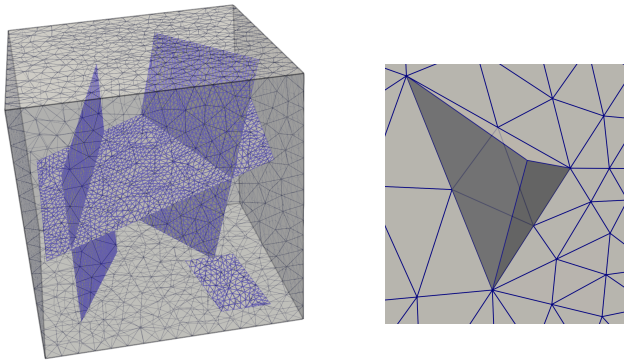

Figure 4: Polytopal mesh of the 3D DFM with roughly 47k cells and 6k fracture faces and obtained from an initial tetrahedral mesh refined along the fracture network by cutting each fracture face in four triangle (left). Example of a polyhedral cell with a tetrahedral shape but 7 faces and 7 nodes as a consequence of the refinement along the fracture network (right).

β_0^n/μ	1	5	10	50	100	100	200	800
β_0^τ/μ	0.4	2	4	20	10	40	80	320
$\theta = -1$	7	8	9	13	16	18	26	81
$\theta = 0$	6	8	9	13	16	18	26	NCV
$\theta = 1$	NCV	8	9	14	15	20	32	NCV

Table 1: Number of Newton iterations obtained on the 47k cells mesh for different values of Nitsche's parameters θ, β_0^n, β_0^τ. NCV means that the converge is not achieved after 300 iterations.

$\#\mathcal{M}$	45k		127k		250k	
Schemes	VB	VN	VB	VN	VB	VN
DOFs	28k	14k	63k	33k	117k	64k
Newton	18	16	19	18	23	23
CPU (s)	3918	2156	25k	12k	139k	84k

Table 2: Performance of the nonlinear solver in terms of number of iterations and CPU time for both the VEM Nitsche (VN) and VEM-bubble (VB) discretisations on the family of meshes. Nitsche's parameters are fixed to $\theta = -1$, $\beta_0^n = 100\mu$, $\beta_0^\tau = 10\mu$.

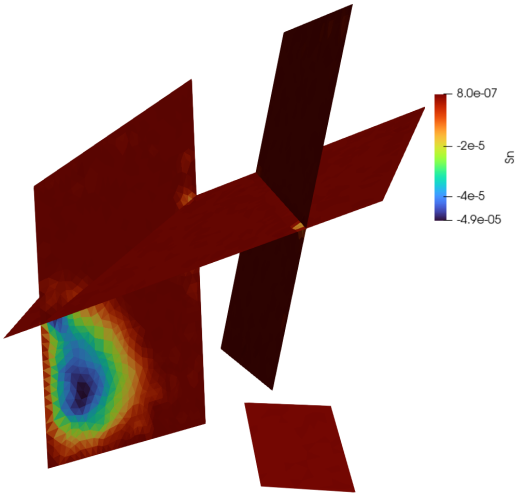

(a) VN 47k, $\frac{\beta_0}{\mu} = (100, 10)$

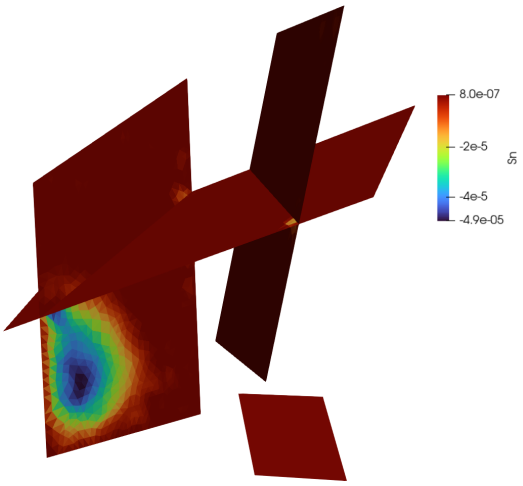

(b) VB 47k

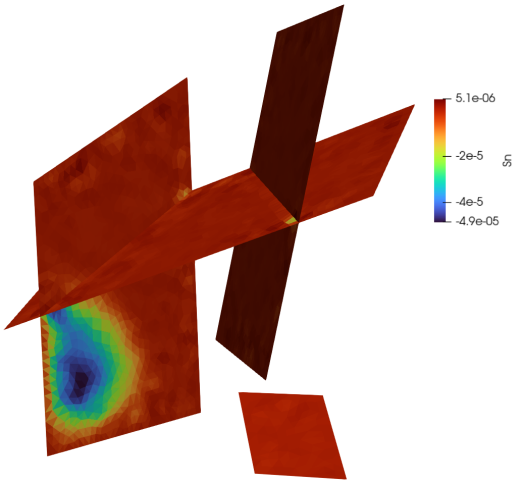

(c) VN 47k, $\frac{\beta_0}{\mu} = (5, 2)$

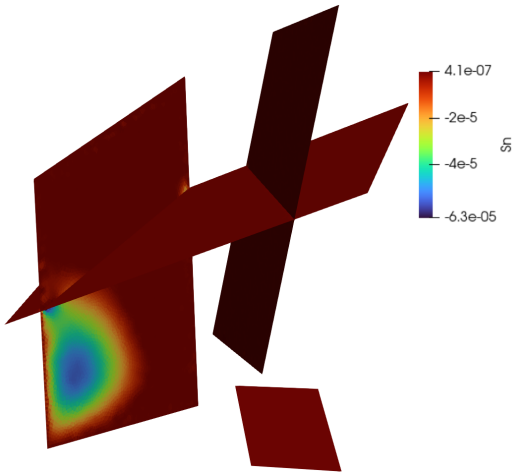

(d) Reference solution

Figure 5: Normal displacement jump for (a) VEM-Nitsche (VN) on the 47k cells mesh with $\frac{\beta_0}{\mu} = (\frac{\beta_0^n}{\mu}, \frac{\beta_0^\tau}{\mu}) = (100, 10)$, (b) VEM-Bubble (VB) on the 47k cells mesh, (c) VEM-Nitsche on the 47k cells mesh with $\frac{\beta_0^n}{\mu} = 5$, $\frac{\beta_0^\tau}{\mu} = 2$, and (d) the reference solution on the 450k cells mesh.

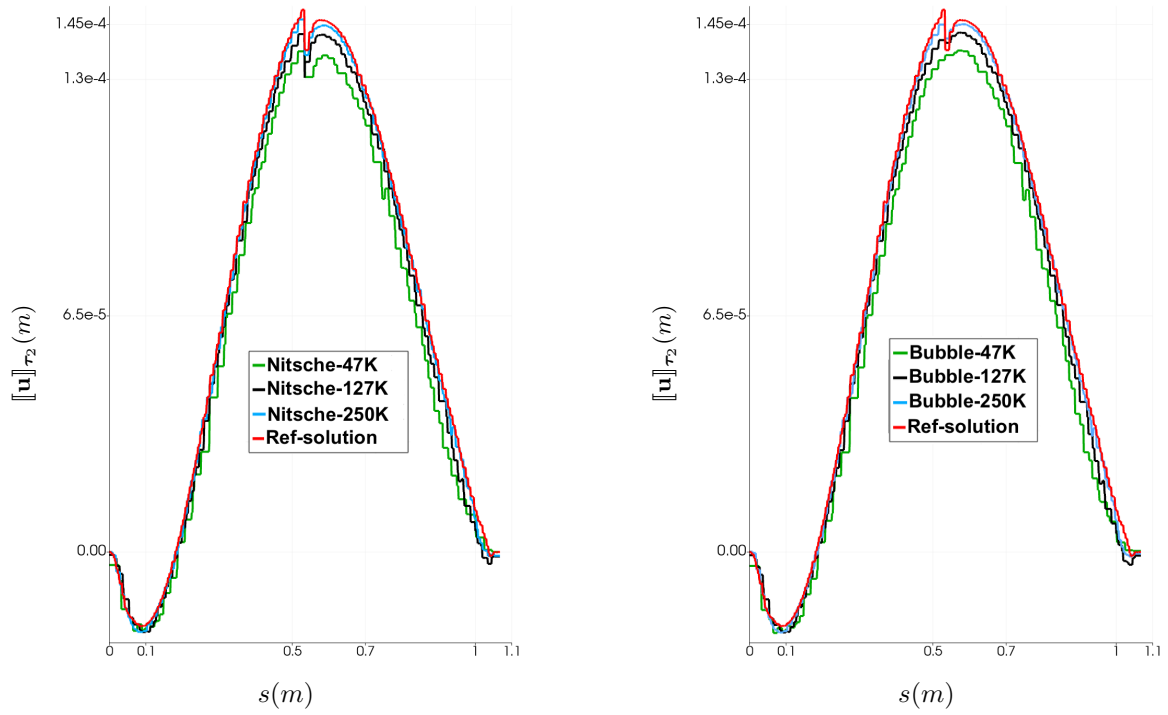

Figure 6: The $\boldsymbol{\tau}_2$ component of the tangential displacement jump along the diagonal line of the right vertical fracture for the 47k, 127k, and 250k meshes, compared with the reference solution, for both VEM-Nitsche's and VEM-Bubble methods. Nitsche's parameters are fixed to $\theta = -1$, $\beta_0^n = 100\mu$, $\beta_0^\tau = 10\mu$.

6 Conclusion

We have presented in this work a first order VEM polytopal discretisation combined with Nitsche's formulation for frictionless contact-mechanics based only on the displacement field nodal unknowns. The numerical analysis, performed in the fully discrete framework, provides an optimal error estimate with minimal regularity assumptions. The discretisation and the analysis account for networks of fractures including corners, tips and intersections. Following [17, 20, 3], the discretisation readily extends to the Mohr-Coulomb frictional model and the numerical analysis to the Tresca friction. Moreover, this approach is naturally suited to semi-smooth Newton nonlinear solvers. Numerical experiments illustrate the theoretical convergence on a manufactured solution and the good numerical behavior of the scheme on a Coulomb frictional model both in terms of CPU time and accuracy compared with the VEM-bubble discretisation. Applications to poromechanical models including fault reactivation by fluid injection will be presented in a forthcoming work.

Acknowledgements: the authors are grateful to Andra and BRGM for partially funding this work and to Jérome Droniou, Laurence Beaude, Marc Leconte, Simon Lopez, Antoine Pasteau and Farid Smai for fruitful discussions during the elaboration of this work.

References

[1] P. Alart and A. Curnier. A mixed formulation for frictional contact problems prone to newton like solution methods. *Computer Methods in Applied Mechanics and Engineering*, 92(3):353–375, 1991.

[2] O. Andersen, H.M. Nilsen, and X. Raynaud. Virtual element method for geomechanical simulations of reservoir models. *Computational Geosciences*, 21(5):877–893, 2017.

[3] L. Beaude, F. Chouly, M. Laaziri, and R. Masson. Mixed and Nitsche's discretizations of coulomb frictional contact-mechanics for mixed dimensional poromechanical models. *Computer Methods in Applied Mechanics and Engineering*, 413:116124, 2023.

[4] Lourenço Beirão da Veiga, Carlo Lovadina, and Alessandro Russo. Stability analysis for the virtual element method. *Mathematical Models and Methods in Applied Sciences*, 27(13):2557–2594, 2017.

[5] L. Beirão Da Veiga, F. Brezzi, and L.D. Marini. Virtual elements for linear elasticity problems. *SIAM Journal on Numerical Analysis*, 51:794–812, 2013.

[6] L Beirão da Veiga, Franco Brezzi, Andrea Cangiani, Gianmarco Manzini, L Donatella Marini, and Alessandro Russo. Basic principles of virtual element methods. *Mathematical Models and Methods in Applied Sciences*, 23(01):199–214, 2013.

[7] L. Beirão Da Veiga, C. Lovadina, and D. Mora. A virtual element method for elastic and inelastic problems on polytope meshes. *Computer methods in applied mechanics and engineering*, 295:327–346, 2015.

[8] F. Ben Belgacem and Y. Renard. Hybrid finite element methods for the signorini problem. *Mathematics of Computation*, 72:1117–1145, 2003.

[9] R. L. Berge, I. Berre, E. Keilegavlen, J. M. Nordbotten, and B. Wohlmuth. Finite volume discretization for poroelastic media with fractures modeled by contact mechanics. *International Journal for Numerical Methods in Engineering*, 121:644–663, 2019.

[10] F. Bonaldi, J. Droniou, R. Masson, and A. Pasteau. Energy-stable discretization of two-phase flows in deformable porous media with frictional contact at matrix-fracture interfaces. *Journal of Computational Physics*, 455:Paper No. 110984, 28, 2022.

[11] A. Borio, F. Hamon, N. Castelletto, J.A. White, and R.S. Settgast. Hybrid mimetic finite-difference and virtual element formulation for coupled poromechanics. *Computer Methods in Applied Mechanics and Engineering*, 383:113917, 2021.

[12] S.C. Brenner and L. R. Scott. *The Mathematical Theory of Finite Element Methods*. Springer-Verlag, New York, 1994.

[13] Susanne C. Brenner, Qingguang Guan, and Li-Yeng Sung. Some estimates for virtual element methods. *Computational Methods in Applied Mathematics*, 17(4):553–574, 2017.

[14] Haïm Brézis. Équations et inéquations non linéaires dans les espaces vectoriels en dualité. *Annales de l'Institut Fourier*, 18(1):115–175, 1968.

[15] E. Burman, P. Hansbo, and M.G. Larson. The augmented Lagrangian method as a framework for stabilised methods in computational mechanics. *Archives of Computational Methods in Engineering*, 30(4):2579–2604, 2023.

[16] Burman, Erik, Hansbo, Peter, and Larson, Mats G. Augmented lagrangian finite element methods for contact problems. *ESAIM: M2AN*, 53(1):173–195, 2019.

[17] F. Chouly. An adaptation of Nitsche's method to the Tresca friction problem. *Journal of Mathematical Analysis and Applications*, 411(1):329–339, 2014.

[18] F. Chouly, A. Ern, and N. Pignet. A hybrid high-order discretization combined with nitsche's method for contact and tresca friction in small strain elasticity. *SIAM Journal on Scientific Computing*, 42(4):A2300–A2324, 2020.

[19] F. Chouly and P. Hild. A Nitsche-based method for unilateral contact problems: numerical analysis. *SIAM Journal on Numerical Analysis*, 51(2):1295–1307, 2013.

[20] F. Chouly, P. Hild, V. Lleras, and Y. Renard. Nitsche method for contact with coulomb friction: Existence results for the static and dynamic finite element formulations. *Journal of Computational and Applied Mathematics*, 416:114557, 2022.

[21] F. Chouly, P. Hild, and Y. Renard. Symmetric and non-symmetric variants of Nitsche's method for contact problems in elasticity: theory and numerical experiments. *Mathematics of Computation*, 84(293):1089–1112, 2015.

[22] F. Chouly, P. Hild, and Y. Renard. *Finite Element Approximation of Contact and Friction in Elasticity*. Birkhäuser Cham, 2023.

[23] M. Cihan, B. Hudobivnik, J. Korelc, and P. Wriggers. A virtual element method for 3d contact problems with non-conforming meshes. *Computer Methods in Applied Mechanics and Engineering*, 402:115385, 2022. A Special Issue in Honor of the Lifetime Achievements of J. Tinsley Oden.

[24] J. Coulet, I. Faille, V. Girault, N. Guy, and F. Nataf. A fully coupled scheme using virtual element method and finite volume for poroelasticity. *Computational Geosciences*, 24:381–403, 2020.

[25] D. Di Pietro and S. Lemaire. An extension of the Crouzeix-Raviart space to general meshes with application to quasi-incompressible linear elasticity and Stokes flow. *Mathematics of Computation*, 84:1–31, 2015.

[26] D.A. Di Pietro and J. Droniou. *The Hybrid High-Order Method for Polytopal Meshes: Design, Analysis, and Applications*, volume 19 of *Modeling, Simulation and Applications*. Springer International Publishing, 2020.

[27] Daniele Antonio Di Pietro and Alexandre Ern. *Mathematical Aspects of Discontinuous Galerkin Methods*, volume 69 of *Mathématiques et Applications*. Springer-Verlag, January 2012.

[28] J. Droniou, G. Enchéry, I. Faille, A. Haidar, and R. Masson. A bubble vem–fully discrete polytopal scheme for mixed-dimensional poromechanics with frictional contact at matrix-fracture interfaces. *Computer Methods in Applied Mechanics and Engineering*, 422:116838, 2024.

[29] J. Droniou, A. Haidar, and R. Masson. Analysis of a VEM-fully discrete polytopal scheme with bubble stabilisation for contact mechanics with Tresca friction. preprint https://hal.science/hal-04542460, April 2024.

[30] G. Drouet and P. Hild. An accurate local average contact method for nonmatching meshes. *Numerische Mathematik*, 136(2):467–502, 2017.

[31] G. Enchéry and L. Agélas. Coupling linear virtual element and non-linear finite volume methods for poroelasticity. *Comptes Rendus. Mécanique*, 2023. Online first.

[32] R. Eymard, T. Gallouët, and R. Herbin. Discretization of heterogeneous and anisotropic diffusion problems on general nonconforming meshes sushi: a scheme using stabilization and hybrid interfaces. *IMA Journal of Numerical Analysis*, 30(4):1009–1043, 2010.

[33] A. Franceschini, N. Castelletto, J.A. White, and H.A. Tchelepi. Algebraically stabilized Lagrange multiplier method for frictional contact mechanics with hydraulically active fractures. *Computer Methods in Applied Mechanics and Engineering*, 368:113161, 2020.

[34] P. Hansbo and M.G. Larson. Discontinuous Galerkin and the Crouzeix–Raviart element: Application to elasticity. *ESAIM: Mathematical Modelling and Numerical Analysis*, 37:63–72, 2003.

[35] J. Haslinger, I. Hlaváček, and J. Nečas. *Numerical methods for unilateral problems in solid mechanics*, volume IV of *Handbook of Numerical Analysis (eds. P.G. Ciarlet and J.L. Lions)*. North-Holland Publishing Co., Amsterdam, 1996.

[36] Patrick Hild and Yves Renard. A stabilized lagrange multiplier method for the finite element approximation of contact problems in elastostatics. *Numerische Mathematik*, 115(1):101–129, 2010.

[37] Thomas J.R. Hughes and Leopoldo P. Franca. A new finite element formulation for computational fluid dynamics: Vii. the stokes problem with various well-posed boundary conditions: Symmetric formulations that converge for all velocity/pressure spaces. *Computer Methods in Applied Mechanics and Engineering*, 65(1):85–96, 1987.

[38] E. Keilegavlen and J.M. Nordbotten. Finite volume methods for elasticity with weak symmetry. *International Journal for Numerical Methods in Engineering*, 112:939–962, 2017.

[39] M. Laaziri, R. Masson, and A. Haidar. VEM–Nitsche Fully Discrete Polytopal Scheme for Mixed-Dimensional Poromechanical Models with Coulomb Frictional Contact at Matrix-Fracture Interfaces. In *ECMOR 2024 Proceedings*, pages 1–9. European Association of Geoscientists & Engineers, 2024.

[40] V. Lleras. A stabilized Lagrange multiplier method for the finite element approximation of frictional contact problems in elastostatics. *Mathematical Modelling of Natural Phenomena*, 4(1):163–182, 2009.

[41] F. Wang and B.D. Reddy. A priori error analysis of virtual element method for contact problem. *Fixed Point Theory and Algorithms for Sciences and Engineering*, 2022(1):10, 2022.

[42] B. Wohlmuth. Variationally consistent discretization schemes and numerical algorithms for contact problems. *Acta Numerica*, 20:569–734, 2011.

[43] P. Wriggers, F. Aldakheel, and B. Hudobivnik. *Virtual Elements for Fracture Processes*, pages 243–315. Springer International Publishing, Cham, 2024.

[44] P. Wriggers, W.T. Rust, and B.D. Reddy. A virtual element method for contact. *Computational Mechanics*, 58(6):1039–1050, 2016.

[45] Bangmin Wu, Fei Wang, and Weimin Han. Virtual element method for a frictional contact problem with normal compliance. *Communications in Nonlinear Science and Numerical Simulation*, 107:106125, 2022.